# The Effects of Roughness on Turbulent Boundary Layers

by

Fanxiao Meng

A Thesis submitted to the Faculty of Graduate Studies of

The University of Manitoba

in partial fulfillment of the requirements of the degree of

MASTER OF SCIENCE

Department of Mechanical Engineering

University of Manitoba

Winnipeg

# ABSTRACT

In this thesis, the effects of roughness on turbulent boundary layers are investigated by both the experimental and analytical methods. Two aspects of roughness are investigated, including the similarity between the smooth and rough turbulent boundary layers, and the characteristics of the flow over the step changes in roughness. Based on the data from the thesis of Akinlade (2005), the validity of three different kinds of outer scales is examined for the defect law in the context of smooth surface and three different types of rough surfaces. Furthermore, a mathematical relation is derived to further investigate the roughness effects. For the second topic, experiments were performed on a smooth-rough-smooth transition in a wind tunnel using a boundary layer Pitot tube. In addition, the growth rates of internal boundary layer thicknesses are determined using the method of Antonia and Luxton (1971, 1972), and the results are compared with the previous studies.

# ACKNOWLEDGEMENTS

Firstly, I would like to express my gratitude to my supervisors, Professor Donald J. Bergstrom and Professor Bing-Chen Wang for offering me a valuable opportunity to pursue my M.Sc. program at the University of Manitoba and University of Saskatchewan. I would also profoundly thank them for their consistent financial support and academic advice.

I am grateful to Professor David Sumner and Mr. Dave Deutsher for their assistance and help during my experiments. I would like to thank my all friends and student colleagues met in Winnipeg and Saskatoon, Ye Zhang, Xingjun Fang, Mohammad Saeedi, Shahin Nasseri Oskouie, Zixuan Yang and Qianqiu Xun. Thank you for your help, friendship and many joyful and memorable moments.

Thanks to the all the past I experienced, without them I cannot become the person I am today.

Thanks to my fiancée, Ying Li. Thank the destiny for letting us meet.

At last, but not least, I would like to express the deepest gratitude to my parents. You give me my life and a home. You are like a haven for me, and you always support me at back wherever I am. You mean the whole world to me, and you are my faith for the future.

*To my parents*

*To my fiancée, Ying Li*

*To the destiny and to my faith*

# TABLE OF CONTENTS

# LIST OF TABLES

# LIST OF FIGURES

# NOMENCLATURE

## English Symbols

$B$ : A constant in the Log Law

$c_0$ : A nonzero constant which is equal to the area under the curves when integrating the defect law

$f_i$ : Non-dimensional function for the inner layer

$f_o$ : Non-dimensional function for the outer layer

$H$ : Shape factor

$h$ : A non-dimensional parameter indicating the location in $y$ direction between the surface and the boundary layer edge

$k$ : Roughness height (mm)

$k_s$ : Equivalent sand grain roughness height (mm)

$k_s^+$ : Equivalent sand grain roughness Reynolds number ($k_s u_\tau / \nu$)

$Re_\theta$ : Reynolds number based on momentum thickness (mm)

$U$ : Mean streamwise velocity (m/s)

$U_e$ : Freestream velocity (m/s)

$\langle u_i u_j \rangle$ : Turbulent shear stress tensor ($m^2/s^2$)

$u_o$ : Velocity scale for the outer layer (m/s)

$u_\tau$ (or $u_*$) : Friction velocity (m/s)

$u_{*1}$ : Friction velocity on the upwind surface (m/s)

$u_{*2}$ : Friction velocity on the downwind surface (m/s)

$x$ : Streamwise coordinate direction (mm)

$x_1$ : Origin of the smooth-rough transition

$x_2$ : Origin of the rough-smooth transition

$y$ : Wall-normal coordinate direction (mm)

$z_0$ : Aerodynamic Roughness length (mm)

$z_{01}$ : Upwind surface roughness length (mm)

$z_{02}$ : Downwind surface roughness length (mm)

$z_{0R}$ : Roughness length of the rough surface (mm)

$z_{0S}$ : Roughness length of the smooth surface (mm)

# Greek Symbols

$\alpha$ : A parameter representing the upstream condition

$\Delta U^+$ : Roughness shift in the Log Law

$\delta$ : Boundary layer thickness (mm)

$\delta^*$ : Displacement thickness (mm)

$\delta^+$ : Reynolds number based on boundary layer thickness

$\delta_i$ : Internal boundary layer thickness (mm)

$\theta$ : Momentum thickness (mm)

$\kappa$ : von Kármán constant

$\nu$ : Kinematic viscosity ($m^2/s$)

$\Pi$ : Strength of the wake

$\rho$ : Density ($kg/m^3$)

$\tau_s$ : Surface shear stress ($N/m^2$)

$\tau_{s1}$ : Surface shear stress on the upwind surface ($N/m^2$)

$\tau_{s2}$ : Surface shear stress on the downwind surface ($N/m^2$)

# Abbreviations

HSTS : High-speed test section

IBL : Internal Boundary Layer

LSTS : Low-speed test section

PL : Perforated steel sheet rough surface

SG : Sand grain rough surface

SM : Smooth surface

WM : Wire mesh rough surface

ZPG : Zero pressure gradient

ZS-scaling : The outer scale proposed by Zagarola and Smits (1998)

# 1 INTRODUCTION

## 1.1 Turbulent Flows and Turbulent Boundary Layer

Turbulent flows is one of the most frequently observed phenomena in our everyday life, such as the water flowing in a river, airflow around a plane and car, wind blowing in a city and so on. Turbulent flows play an important role in various industrial applications, and it transports and mixes fluid much more effectively than laminar flows. Turbulent flow phenomenon represents one of the most complex and challenging subjects in natural science and engineering.

There are many different techniques to study turbulent flows, and according to Pope (2000), the study of turbulent flows can be generally classified into the following three categories:

(1) Discovery: experimental or simulation studies aimed at providing qualitative or quantitative information about particular flows.

(2) Modeling: theoretical or modeling studies aimed at developing tractable mathematical models that can accurately predict properties of turbulent flows.

(3) Control: studies aimed at manipulating or controlling the turbulence in a beneficial way.

The concept of the boundary layer was first introduced by Ludwig Prandtl in 1904, who showed that the effects of the friction within the fluid are confined to a very thin layer close to the surface. The boundary layer thickness can be quantitatively determined in many ways. Based on his laboratory research, Schlichting (1979) stated that the boundary layer thickness, $\delta$, has often been defined as the wall normal distance above which the change of velocity from the freestream value is less than 1 %. However, this criterion based on 1 % of mean velocity difference is

arbitrary and such a small difference is difficult to determine in a field work. Therefore, larger criteria, such as 5 or 10 %, have also been used in literature.

Since a turbulent boundary layer is more complex and more commonly encountered in engineering practice than a laminar boundary layer, the study of the turbulent boundary layer is more challenging and more relevant to industrial applications.

## 1.2 Structure of Turbulent Boundary Layer

The turbulent boundary layer subjected to a zero pressure gradient (ZPG) typically consists of two regions, i.e., the inner and outer layers, which are illustrated in Figure 1.1. In the figure, the fine vertical structure of the turbulent boundary layer is demonstrated. In general, the turbulent boundary layer consists of viscous sublayer, meso layer, inertial layer and outer boundary layer. The inner and outer layer studied in this thesis refers specifically to the regions that can be described using the inner and outer layer equations, respectively. Early in 1932, Prandtl stated that the viscosity ($\nu$) and the surface shear stress ($\tau_s$) are the significant parameters which influence the mean velocity profiles in the inner layer, such that

$$U = f_i\left(u_\tau, \nu, y\right) \tag{1.1}$$

where $U$ is the mean velocity, $u_\tau$ is the friction velocity, defined as $u_\tau = \sqrt{\tau_s/\rho}$ ($\rho$ is the density), $y$ is the distance in wall-normal direction and $f_i$ is a function for the inner layer.

For the outer layer, the viscosity has little effects on the velocity profiles compared to the turbulent mixing at sufficiently high Reynolds number, and so, the outer equation can be written as

$$U = f_o\left(u_o, y, \delta\right) \tag{1.2}$$

where $f_o$ is a function for the outer layer and $u_o$ is the velocity scale for the outer layer.

From dimensional analysis, Eqs. (1.1) and (1.2) lead to the following dimensionless relations:

$$U^+ = f_i\left(y^+\right) \tag{1.3}$$

and

$$\frac{U_e - U}{u_o} = f_o\left(\frac{y}{\delta}\right) \tag{1.4}$$

where, $U^+ = U/u_\tau$ , $y^+ = yu_\tau/\nu$ and $U_e$ is the freestream velocity. Eq. (1.3) is the classical Law of the Wall for the inner layer and Eq. (1.4) is the Defect Law for the outer layer. Both of these relations assume complete similarity, which means that if one proper scale is used, the mean velocity profiles of different flows collapse to one single curve. Otherwise, for the incomplete similarity， different mean velocity profiles cannot collapse no matter the form of scales is in use.

Millikan (1938) proposed that an overlap region exists between the inner and outer layers at sufficiently high Reynolds numbers. By combining Eqs. (1.3) and (1.4), the famous Log Law is obtained for the overlap region, in the form of

$$U^+ = \frac{1}{\kappa}\ln y^+ + B \tag{1.5}$$

where $\kappa$ is the von Kármán constant, and $B$ is a constant which depends on the surface condition. Eq. (1.5) is typically used to determine the value of the friction velocity on the surface and evaluate the effects of roughness.

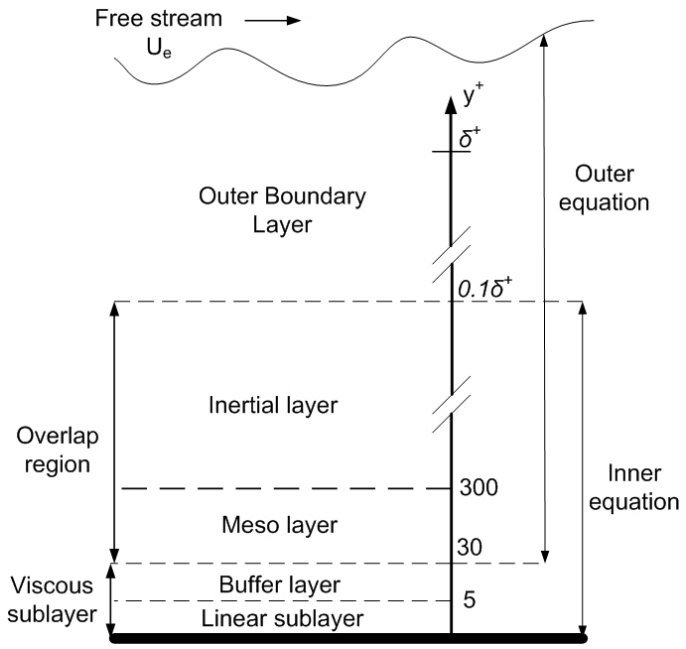


Figure 1.1: Schematic of the structure of a turbulent boundary layer.
($\delta^+ (= \delta u_\tau/\nu)$ is the Reynolds number based on boundary layer thickness.)

## 1.3 Effects of Roughness on Turbulent Boundary Layer

Surface roughness can have profound effects on the turbulent boundary layer. For instance, roughness can increase the skin friction at the wall and accordingly change the mean velocity profile. Depending on the value of the equivalent sand grain roughness Reynolds number, $k_s^+$, Schlichting (1979) proposed three flow regimes existing for turbulent flow over a rough surface: hydraulically smooth ($k_s^+ < 5$), transitionally rough ($5 \leq k_s^+ \leq 70$) and fully rough ($k_s^+ > 70$).

Note that $k_s^+ = k_s u_\tau/\nu$ and $k_s$ is the height of monodisperse, uniformly packed sand grain required to produce the equivalent roughness effects as the actual roughness elements.

For a fully-developed turbulent boundary layer, the effects of the roughness can be evaluated using the so-called roughness shift ($\Delta U^+$) in the Log Law, as illustrated in Figure 1.2. According to Perry *et al.* (1969), based on the flow characteristics and the roughness shift, the roughness elements can be classified into two types: *k*-type and *d*-type. If the roughness shift depends on the roughness height *k*, it is called a *k*-type roughness element. If the cavities between the roughness elements are narrow, and the roughness shift depends on an outer scale, such as the pipe diameter, it is referred to as *d*-type.

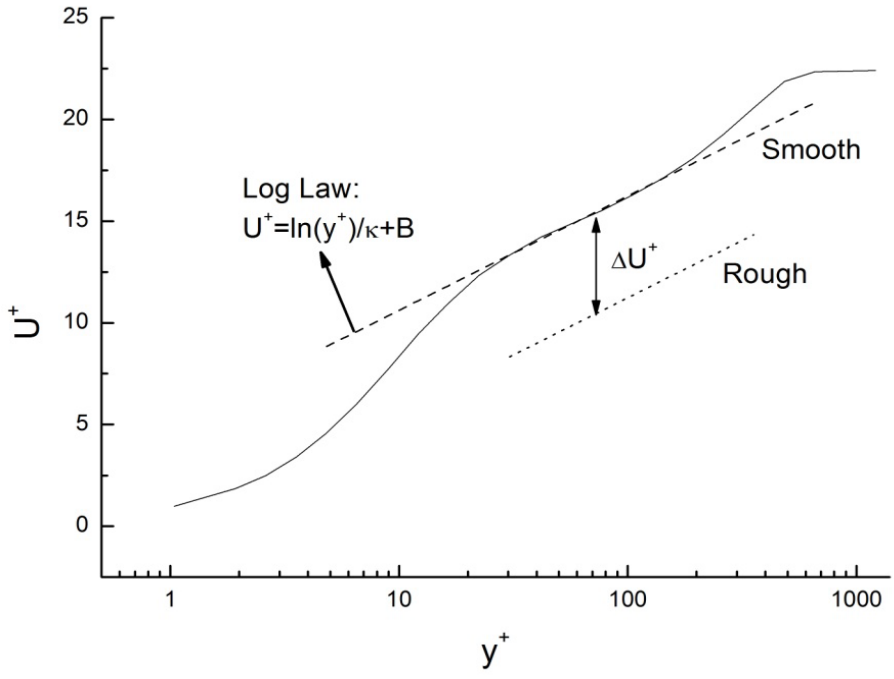


Figure 1.2: Schematic of the effects of roughness on the mean velocity profile in the inner coordinates.

One problem about roughness effects is if the similarity holds between smooth and rough turbulent boundary layers in the outer region. According to the wall similarity hypothesis of Townsend (1980), when appropriately scaled, the turbulent flow outside the roughness sublayer is not affected by wall roughness at a sufficiently high Reynolds number. This means the effect of roughness is confined to the bottom of the inner layer and complete similarity is expected in the outer layer.

Another issue related to roughness effects is how the flow is influenced by the step changes in roughness. The main characteristic of the flow after step changes in roughness is the development of an Internal Boundary Layer (IBL) which refers to the region where the flow is influenced by a new surface condition. Investigation of the development of an IBL provides insights into how the flow adjusts to the new surface condition after a step change in roughness and whether or not the turbulent boundary layer is able to re-establish an equilibrium condition in the context of a new local surface.

In this context, this research addresses the following two important questions:

(1) Does the effect of surface roughness extend into the outer layer, which would imply that smooth- and rough-wall turbulent boundary layers are not similar in the outer region?

(2) How does a turbulent boundary layer develop after passing over two step changes in surface roughness created by a local region of sandpaper roughness on a smooth plate?

## 1.4 Objectives and Organization of the Thesis

In order to answer the two important questions listed in Chapter 1.3, both experimental and theoretical methods are used in this study. Correspondingly, this thesis mainly consists of two parts: one is about the similarity of the smooth and rough boundary layers, and the other is on the IBL development after a roughness step change. Through these two aspects of studies, the effects of roughness on turbulent boundary layers are thoroughly investigated, and some new conclusions, which challenge some of the classical comcepts, are obtained.

In Chapter 2, a thorough literature review about the similarity between smooth and rough turbulent boundary layers and models of IBLs is presented.

In Chapter 3, the experimental set-up and testing conditions are described.

In Chapter 4, based on the assumption of complete similarity between smooth and rough surface boundary layers, a mathematical derivation of the scale for the mean velocity defect law is presented. Subsequently, this proposed method is applied to analysis of experimental data obtained in a wind tunnel to examine the effectiveness of the Zagarola-Smits (ZS) scaling approach, and the similarity between smooth and rough turbulent boundary layers.

In Chapter 5, the flow over a smooth-rough-smooth transition in surface roughness is investigated experimentally in a wind tunnel by measuring the mean velocity profiles at different streamwise locations, and the mean velocity profiles clearly demonstrate how the flow develops after two continuously step changes in roughness. Subsequently, the mean velocity profiles are used to determine the IBL thickness and the growth rates of the IBL thicknesses. The obtained results are compared with the previous studies.

Finally, in Chapter 6, major conclusions of this thesis research and discussions of future studies are presented.

# 2 LITERATURE REVIEW

## 2.1 Similarity of Turbulent Boundary Layers

### 2.1.1 Similarity between Smooth and Rough Turbulent Boundary Layers

An important issue related to the effect of surface roughness on the turbulent boundary layer is the outer layer similarity between smooth- and rough-wall turbulent boundary layers. Patel (1998) indicated that the question of outer layer similarity is of practical interest since most computational models for rough walls rely at some level on the similarity between smooth and rough wall flows. Clauser (1954) and Hama (1954) found that the effect of surface roughness on the mean flow is confined to the inner layer, causing a downward shift in the Log Law, called the roughness function ($\Delta U^+$) and they suggested that the mean velocity in the outer region expressed in velocity-defect form should be independent of surface roughness. According to the wall similarity hypothesis of Townsend (1980), the turbulent flow outside the roughness sublayer is not affected by wall roughness at a sufficiently high Reynolds number. Following Perry and Abell (1977), this implies that a rough-wall boundary layer at sufficiently high Reynolds numbers is structurally similar to that on a smooth surface outside the roughness sublayer.

The validity of the wall similarity hypothesis between smooth- and rough-wall boundary layers has been investigated through the study of the mean velocity profile and higher order turbulence statistics. Some investigations support the hypothesis that the effects of roughness are confined within the inner layer. Raupach *et al.* (1991) concluded that flow structures are unaffected by surface roughness in the outer region of the shear layer, which observation supports the wall

similarity hypothesis of Townsend (1980). This viewpoint was further confirmed by Krogstad *et al.* (1992). The study of Flack *et al.* (2005) shows support for outer layer similarity in both the mean flow and turbulence statistics for both smooth and rough walls.

On the other hand, other studies concluded that even in the outer layer, the structures of smooth and rough wall boundary layers are not similar, which implies that the roughness effects extend into the outer layer. Relevant literatures on this viewpoint are represented by Keirsbulck *et al.* (2002), Tachie *et al.* (2003), and Akinlade *et al.* (2004). Jiménez (2004) indicated that the outer similarity depends on the ratio between the boundary layer thickness, $\delta$, and the roughness height, $k$. Similarity only exists if $k$ is sufficiently small compared to $\delta$, i.e., $\delta/k \geq 40$.

Related to the debate on similarity between smooth- and rough-wall turbulent boundary layers, there is a second question on whether similarity exists between different kinds of rough wall boundary layers. Characterising wall roughness is difficult, since the geometry and length scales of the roughness elements vary widely. Furthermore, the roughness encountered in industrial applications is typically more complicated than the two-dimensional (2-D) regularly spaced roughness and three-dimensional (3-D) uniformly distributed roughness used in the laboratory research. Krogstad and Antonia (1999) pointed out that although very different surface geometries may produce the same effect on the mean velocity profile, the turbulence generation mechanisms may differ substantially. Inspired by the previous studies, this thesis further investigates the effects of roughness elements with different geometries on the mean velocity profiles.

### 2.1.2 Outer Velocity Scales for the Defect Law

The similarity of the mean velocity profiles in the outer layer can be assessed using velocity-defect scaling. Connelly *et al.* (2006) pointed out that for smooth- and rough-wall turbulent boundary layers, collapse of the mean velocity profiles usually indicates that roughness effects on the mean flow are confined within the inner layer. Lack of collapse typically results in propagation of roughness effects into the outer region of the boundary layer. In literature, three different velocity scales are commonly used to nondimensionlise the velocity defect profiles in

Table 1.1: A summary of the velocity scales for the inner and outer layers.

| Investigator | Quantity | Inner | Outer |
|---|---|---|---|
| **Classical** | $U$ | $u_\tau$ | $u_\tau$ |
| **GC 97** | $U$ | $u_\tau$ | $U_e$ |
| **ZS 98** | $U$ | $u_\tau$ | $U_e \frac{\delta^*}{\delta}$ |
| **Classical** | $\langle u^2 \rangle$ | $u_\tau^2$ | $u_\tau^2$ |
| **Classical** | $\langle v^2 \rangle$ | $u_\tau^2$ | $u_\tau^2$ |
| **Classical** | $\langle uv \rangle$ | $u_\tau^2$ | $u_\tau^2$ |
| **GC 97** | $\langle u^2 \rangle$ | $u_\tau^2$ | $U_e^2$ |
| **GC 97** | $\langle v^2 \rangle$ | $u_\tau^2$ | $U_e^2$ |
| **GC 97** | $\langle uv \rangle$ | $u_\tau^2$ | $U_e^2 \frac{d\delta}{dx}$ |

boundary layers: i.e., the classical friction velocity, $u_\tau$; the freestream velocity, $U_e$, proposed by George and Castillo (1997); and the quanitity, $U_e \frac{\delta^*}{\delta}$, proposed by Zagarola and Smits (1998), hereafter referred to as the ZS-scaling, where $\delta^*$ is the displacement thickness. A comprehensive summary of the velocity scales in the inner and outer layers for both the mean velocity and the

Reynolds stress components is presented in Table 1.1. In the table, the research paper by George and Castillo (1997) is designated as GC 97, and that by Zagarola and Smits (1998) is designated as ZS 98.

In this thesis, all these three outer velocity scales, i.e., $u_\tau$, $U_e$ and $U_e \frac{\delta^*}{\delta}$, are used to scale the mean velocity defect profiles in order to investigate the similarity between the smooth- and rough-wall turbulent boundary layers.

## 2.2 Flow over a Step Change in Roughness

### 2.2.1 Practical Significance

The question on how a turbulent boundary layer develops after a step change in roughness is relevant to both environmental and industrial flows. For instance, the wind flowing over ocean-to-land and land-to-lake boundaries are typical examples of smooth-to-rough and rough-to-smooth transitions. In industrial duct systems, surface roughness may occur in localized regions of the wall. Laursen *et al.* (1994) noted that this type of flow also relates to scour protection of structures in coastal areas. Protection of structures resting on the seabed often consists of a stone layer laid on the bed around the structure. In this situation, there will be a step change in roughness between the original seabed and the stone layer. In order to select a safe size of the stones for the protection, an engineer must know the increase in the bed friction due to the step change in roughness. In view of this, improved knowledge of the behavior of the turbulent boundary layer as it experiences a step change in roughness remains as an interesting research topic of practical interests.

Due to the importance of this problem, extensive researches have been conducted through theoretical analysis (Elliott (1958), Panofsky and Townsend (1964), Jackson (1976), Panofsky and Dutton (1984)), experiments (Bradley (1968), Pendergrass and Arya (1984), Cheng and Castro (2002)) and numerical simulations (Peterson (1969), Shir (1972), Rao *et al.* (1974)) over the past several decades. The following sections briefly review some of the major results of these studies.

### 2.2.2 Definition of Internal Boundary Layer

The major feature of turbulent flows over a step change in roughness is the generation of an IBL. In general terms, an IBL is considered to be the region where the flow is influenced by the new surface condition. This layer is generated at the transition of the step changes in roughness and grows with distance in the streamwise direction. When the flows encounter the new surface, the fluid close to the surface first experiences the impact of roughness change, and then the effect propagates upwards. However, Garratt (1990) noted that the definition of the IBL was not always precise and the choice of the IBL definition criteria has typically been determined by practical rather than theoretical considerations. Until now, there is not one commonly accepted method to define the IBL quantitatively, i.e., the IBL thickness.

Figure 2.1 shows a schematic drawing that describes the structure of a two-dimensional IBL developed over two adjacent different types of surfaces. In the figure, the part of the flow adjacent to the surface where the influence of the new surface condition is present is termed as the IBL. Savelyev and Taylor (2005) divided the general structure of the flow after a change in surface conditions into three parts, consisting of an equilibrium layer immediately above the surface, a transition layer and an outer region of incoming flow formed above the old surface.

The IBL comprises the first two layers. Logan and Fichtl (1975) indicated that the IBL interface separates the internal and outer regions. For the rough-smooth transition, the IBL begins at the ground and comprises the accelerating fluid, while the outer region extends up to unmodified flow and comprises decelerating fluid. Jegede and Foken (1999) utilized this concept to analyze their experimental data from the LINEX field studies.

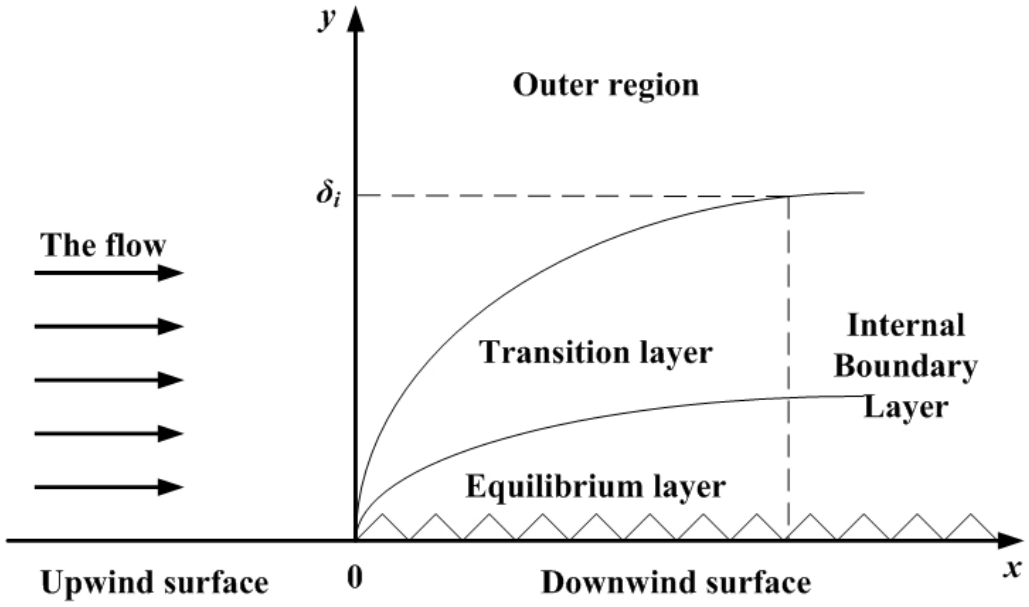


Figure 2.1: A sketch of a two-dimensional IBL.

### 2.2.3 Theoretical Models of Internal Boundary Layer

There are many excellent theoretical works about the development of the IBL. The simplest and most common analytical models were introduced by Elliot (1958) and Panofsky and Townsend (1964). Their models were obtained, respectively, by assuming a constant and a linear vertical distribution of the friction velocity within the IBL.

Elliott (1958) assumed that the downwind velocity profile is in equilibrium with the new surface. Therefore, the velocity profile follows a logarithmic profile all the way up to the IBL height, $\delta_i$. So the mean velocity profile should be of the form:

$$U = \frac{u_{*2}}{\kappa} \ln\left(\frac{y}{z_{02}}\right) \qquad (2.1)$$

where, $U$ is the average velocity at the elevation $y$, $u_{*2}$ is the friction velocity over the downwind surface, $z_{02}$ is the downwind surface roughness length and $\kappa$ is the von Kármán constant. In fact, this equation can be derived by assuming a constant shear stress along the vertical direction for $y < \delta_i$. In order to predict the time-averaged surface shear stress on the downwind surface, $\tau_{s2}$, the following relation can be used:

$$\tau_{s2} = \rho\left[\frac{\kappa U}{\ln\left(\frac{y}{z_{02}}\right)}\right]^2 \qquad (2.2)$$

where $\tau_{s2} = \rho u_{*2}^2$.

A problem associated with this model is that due to a constant vertical turbulent shear stress assumption in use, it produces an unrealistically sharp stress discontinuity at the top of the IBL $y = \delta_i$.

For the IBL thickness $\delta_i$, Elliott (1958) proposed that

$$\left(\frac{\delta_i}{z_{02}}\right) = \left(0.75 - 0.03M'\right)\left(\frac{x}{z_{02}}\right)^{0.8} \qquad (2.3)$$

where $M' = ln\left(\frac{z_{02}}{z_{01}}\right)$, and $z_{01}$ and $z_{02}$ are the upwind and downwind aerodynamic surface roughness length, respectively, and $x$ is the streamwise distance from the roughness change.

To avoid an abrupt change in the surface shear stress at the IBL height $\delta_i$, Panofsky and Townsend (1964) assumed a linear variation of the friction velocity with respect to height within the IBL, viz.

$$u_* = u_{*1}\left[1 - S + S\frac{y}{\delta_i}\right] \qquad (2.4)$$

where $S = \frac{u_{*1} - u_{*2}}{u_{*2}}$ is a non-dimensional parameter relating to the change of the surface shear stress, and $u_{*1}$ and $u_{*2}$ are the upwind and downwind friction velocities, respectively.

The relationship between the upwind and downwind surface shear stresses ($\tau_{s1}$ and $\tau_{s2}$) can be derived from the model of Elliott (1958) as follows:

$$\frac{\tau_{s2}}{\tau_{s1}} = \left[1 - \frac{\frac{\kappa U}{u_{*1}} - \ln\left(\frac{y}{z_{02}}\right)}{\frac{y}{\delta_i} - \ln\left(\frac{y}{z_{02}}\right)}\right]^2 \qquad (2.5)$$

Since an explicit estimation for the IBL thickness is required for this model, Panofsky and Townsend (1964) also proposed a relationship for the IBL thickness given by

$$\frac{4\kappa^2\left(\xi - \xi_0\right)}{\eta} = \ln\eta - 5 + \frac{1}{2}M + \frac{4 - \frac{7}{6}M - \frac{1}{4}M^2}{\ln\eta - 1 + \frac{1}{4}M} + \frac{4 + \frac{7}{6}M + \frac{1}{24}M^2 + \frac{1}{16}M^3}{\left(\ln\eta - 1 + \frac{1}{4}M\right)^2} \qquad (2.6)$$

where $\eta = \frac{\delta_i}{z_{02}}$, $\xi = \frac{x}{z_{02}}$, $M = ln\left(\frac{z_{01}}{z_{02}}\right)$ and $\xi_0 = 0$. For the smooth-rough transition, $M = 1.65$, and for the rough-smooth transition, $M = 2.17$.

Since these pioneering works, the IBL models have continued to improve. Jensen (1978) proposed the following expression for the ratio between downwind and upwind shear stresses at $y = \delta_i$ based on Elliott's model:

$$\frac{\tau_{s2}}{\tau_{s1}} = \left[1 - \frac{M}{\ln\left(\frac{\delta_i}{z_{02}}\right)}\right]^2 \qquad (2.7)$$

Garratt (1990) observed the behavior of velocity profiles in the IBL and suggested that they might be described through a modified logarithmic law of the general form

$$U = \frac{u_{*2}}{\kappa}\ln\left(\frac{y}{z_{02}}\right) + f\left(\frac{y}{\delta_i}\right) \qquad (2.8)$$

where the function $f\left(\frac{y}{\delta_i}\right)$ is of the form,

$$f\left(\frac{y}{\delta_i}\right) = \begin{cases} \left(\frac{u_{*1}}{\kappa}\right) ln\left(\frac{y}{z_{01}}\right) - \left(\frac{u_{*2}}{\kappa}\right) ln\left(\frac{y}{z_{02}}\right) & \left(\frac{y}{\delta_i} \geq 1\right) \\ 0 & \left(\frac{y}{\delta_i} \ll 1\right) \end{cases} \qquad (2.9)$$

In the above equations, $f\left(\frac{y}{\delta_i}\right)$ reflects the effect of the boundary condition given by the upstream logarithmic velocity profile at $y/\delta_i$ and the equilibrium logarithmic velocity profile close to the downwind surface.

Recently, Chamorro and Porté-Agel (2009) proposed a new model for the rough-smooth transition, i.e.,

$$U \approx (1-\lambda)\frac{u_{*2}}{\kappa}\ln\left(\frac{y}{z_{02}}\right) + \lambda\frac{u_{*1}}{\kappa}\ln\left(\frac{y}{z_{01}}\right) \qquad (2.10)$$

where $\lambda$ is the weighting parameter ($0 < \lambda < 1$), and $\lambda = \frac{ln\left(\frac{y}{z_{01}}\right)}{ln\left(\frac{\delta_i}{z_{01}}\right)}$.

In this model, the velocity profiles do not follow a logarithmic law within the IBL. In fact, the velocity profiles show a clear logarithmic function related nonlinear behavior that cannot be reproduced by Elliott's log-law model.

Other models of the IBL, such as those of Wood (1982), Savelyev and Taylor (2001), and Weng, *et al*. (2010) exist. A comprehensive review of IBL thickness models can be found in Savelyev and Taylor (2005).

# 3 EXPERIMENTAL SET-UP

The experiments were performed in a closed-return subsonic wind tunnel at the University of Saskatchewan for a Reynolds numbers based on momentum thickness ranging from $Re_\theta = 7{,}720$ to 12,050. The wind tunnel contains two test sections: the Low-Speed Test Section (LSTS) and High-Speed Test Section (HSTS). The experiments in this thesis were performed in the HSTS which is 1.12 m × 0.91 m in the cross section, and approximately 2.00 m long. The side walls are made of plexiglas to facilitate visual inspection of the probe's position. More details about the wind tunnel are available in the thesis of Akinlade (2005).

A boundary layer Pitot tube was used to measure the mean velocity profiles at different streamwise locations, while the freestream velocity was monitored by a Pitot static probe. The data were acquired using a computer with a 1.8 GHz Intel Pentium 4 processor and a data acquisition card. National Instruments LabVIEW software was used for data acquisition and control of the instruments.

For exploring two different aspects of surface roughness effects on a turbulent boundary layer, i.e., the similarity between smooth- and rough-wall boundary layers and the flow over a step change in roughness, two different experiments were performed. The first experiment focused on measuring the mean velocity profile on smooth- and rough-wall boundary layers for different Reynolds numbers. The second experiment focused on measuring the mean velocity profile for flow over a smooth-rough-smooth transition in the surface condition. The data obtained in the first experiment were also supplemented by another data set obtained by Akinlade as part of his PhD thesis research (2005).

### *(a) Experiments on the IBL*

The experimental investigation of the IBL specifically considered a smooth-rough-smooth transition. A trip strip consisting of a metal rod of square cross-section (6 mm × 6 mm) was placed across the width of the board and approximately 100 mm from the leading edge. The location of the trip strip was quite arbitrary, but some testing experiments were performed to ensure the turbulent boundary layer was fully developed before the flow encountered the rough surface using the trip strip at this location. The same trip strip was used in all experiments in order to maintain consistent development of the flow. Additionally, for all the experiments on different kinds of surface conditions (smooth, rough or smooth-rough-smooth transitional), the surface was smooth upstream of the trip strip.

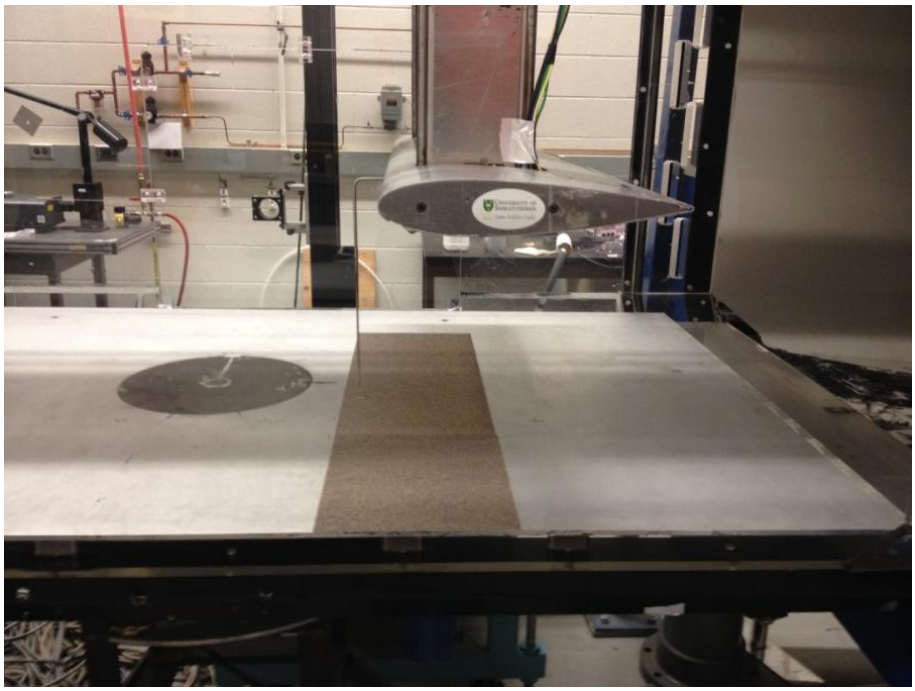

Figure 3.1: The test area in the wind tunnel.

A two-dimensional smooth-rough-smooth transition was created by gluing a section of 40-d grit sandpapers to the ground plane in the test sectio. The sandpaper created a fully rough surface with an equivalent sand grain roughness Reynolds number of $k_s^+$ = 110 calculated from the roughness shift. The length of the sandpaper section was 230 mm, and a boundary layer Pitot tube was used to measure the mean velocity profiles at different streamwise locations, as shown in Figure 3.1. The size of the boundary layer Pitot tube is much thinner than that of the general Pitot tube with a thickness of approximately 0.5 mm, as such, it creates much less intruding effects to the flow.

Figure 3.2 shows a schematic of the measurement domain. Two origins, $x_1$ and $x_2$, were defined based on the two locations where the surface condition abruptly changed. Mean velocity profiles were measured at different locations along the streamwise direction, and for three different freestream velocities, i.e., $U_e$ = 20 m/s, 30 m/s and 40 m/s. For each location, the mean streamwise velocity ($U$) was obtained ranging from next to the surface to the region outside the boundary layer. In the present study, only the mean velocity profiles were measured. Afterwards, the method of Antonia and Luxton (1971, 1972) was applied to obtain determination of the IBL thickness by plotting the mean velocity profiles in the suggested $U/U_e$ vs. $y^{1/2}$ coordinates.

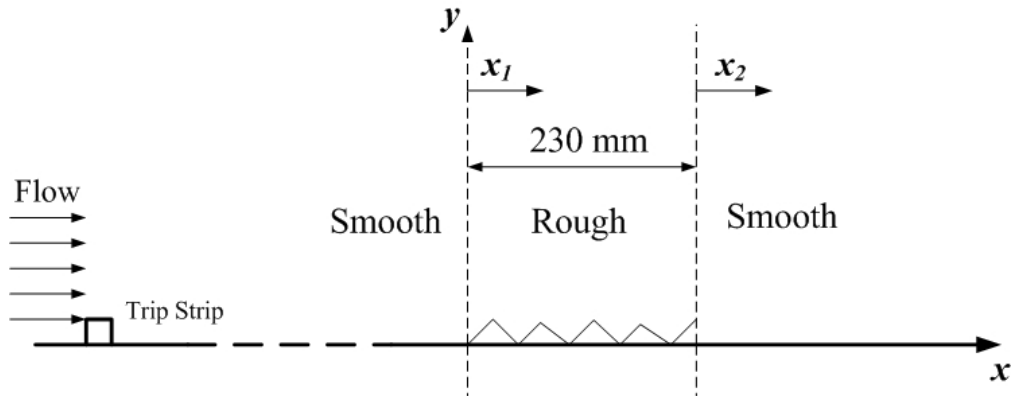


Figure 3.2: Schematic of the testing area.

***(b) Experiments on the Similarity of Turbulent Boundary Layers***

For exploring the similarity of the smooth and rough turbulent boundary layers, select data from the thesis of Akinlade (2005) were used. The smooth surface (SM) was created on a Medium Density Fibre (MDF) board, for which the large-scale deviation was less than ± 0.5 mm from the horizontal plane. The average roughness height for the MDF board was measured which value was 3.82 μm. A turbulent boundary layer was developed on the MDF board mounted on the floor of the wind tunnel. A trip strip made of sand paper (36-d grit) was placed across the width of the board; the trip strip was 75 mm wide and located 15 mm from the leading edge of the board. The trip strip ensured an early transition to turbulence, and was used in all the experiments in order to maintain consistent development of the turbulent boundary layer.

The rough surfaces used in this experiment consisted of the following three roughness elements attached to the MDF board: (i) a sand grain surface (SG) created from 40-d grit sand paper with a roughness height of 0.48 mm; (ii) a 0.9-mm-thick perforated steel sheet (PL) with circular holes, which are 2 mm in diameter and spaced 2.81 mm between centers giving an openness ratio of 45 %; and (iii) a stainless steel woven wire mesh (WM) consisting of 0.36-mm diameter wires laid out with 1.68 mm separation to give an openness ratio of 44 %. In the present study, the thickness of the perforated plate and the diameter of the wire mesh were used to determine the roughness height, $k$. For example, the 0.9 mm thick perforated sheet has a roughness height of $k$ = 0.9 mm, while the woven wire mesh with wire diameter of 0.36 mm has a roughness height of $k$ = 0.72 mm, which is twice the diameter of the wire following Furuya and Fujita (1967). Note that the choice of roughness height is somewhat arbitrary and possibly ambiguous, which however, should not be confused with the equivalent sand grain roughness, $k_s$, calculated from the roughness shift.

Table 3.1 presents a summary of the freestream velocity, $U_e$, Reynolds number based on momentum thickness, $Re_\theta$, Reynolds number based on boundary layer thickness, $\delta^+$, friction velocity, $u_\tau$, blockage ratio, $k/\delta$, strength of the wake, $\Pi$, roughness shift, $\Delta U^+$, roughness Reynolds number, $k^+$, and the equivalent sand grain roughness Reynolds number, $k_s^+$. The equivalent sand grain roughness Reynolds number, $k_s^+$, was obtained from the relation used by Raupach *et al.* (1991). Also following Raupach *et al.* (1991), based on the equivalent sand grain roughness Reynolds number, $k_s^+$, it is clear that fully rough flows were achieved for perforated sheet (PL), sand grain (SG), and wire mesh (WM) surfaces in the experiments.

Table 3.1: Summary of boundary layer parameters.

| | $U_e$ (m/s) | $Re_\theta$ | $\delta^+$ | $u_\tau$ (m/s) | $k/\delta$ | $\Pi$ | $\Delta U^+$ | $k^+$ | $k_s^+$ |
|---|---|---|---|---|---|---|---|---|---|
| SM | 35.9 | 7720 | 2830 | 1.32 | - | 0.520 | - | - | - |
| PL | 35.1 | 9190 | 3660 | 1.80 | 0.026 | 0.557 | 8.3 | 95 | 127 |
| SG | 35.6 | 9790 | 3710 | 1.83 | 0.014 | 0.551 | 8.5 | 51 | 137 |
| WM | 35.6 | 9570 | 4130 | 1.89 | 0.020 | 0.595 | 9.1 | 82 | 177 |

In addition to Akinlade's (2005) data, additional experiments were conducted on the smooth and rough surfaces for different Reynolds numbers. The experimental set-up remained the same as that in the previous section. For the smooth surface, three different freestream velocities were considered, i.e., $U_e$ = 20 m/s, 30 m/s and 40 m/s, while for the rough surface, two freestream velocities were considered, i.e., $U_e$ = 20 m/s, 30 m/s.

### *(c) Uncertainty Estimates*

In order to conduct an uncertainty analysis, the 95 % precision and bias confidence limits were estimated following the approach of Coleman and Steele (2009). Precision uncertainty estimates for the velocity measurements were made through repeatability tests. The systematic error, which represents the bias uncertainty, was obtained from the instrumentation used in the measurements. The estimated bias errors were combined with the precision uncertainties to calculate the overall uncertainties for the measured quantities. The uncertainty in the wall-normal position ($y$) was ± 0.05 mm, and very close to the wall, the uncertainty of the local velocity was approximately 2 %. The uncertainty analysis is presented in Appendix A, and Table 3.2 summarizes the uncertainty estimates for both measured and derived quantities.

Table 3.2: Summary of uncertainty estimates.

| Parameter | Uncertainty estimate |
|---|---|
| Wall-normal position ($y$) | ± 0.05 mm |
| Local velocity ($U$) | ± 2 % |
| *Density ($\rho$) | ± 1.08 % |
| Dynamic viscosity ($\mu$) | ± 0.25 % |
| *Freestream velocity ($U_e$) | ± 0.75 % |
| Boundary layer thickness ($\delta$) | ± 5 % |
| Displacement thickness ($\delta^*$) | ± 5 % |
| Momentum thickness ($\theta$) | ± 5 % |

*Uncertainty estimates from Akinlade (2005).

# 4 SIMILARITY OF TURBULENT BOUNDARY LAYERS

## 4.1 Introduction

One of the most important issues related to the effects of roughness on a turbulent boundary layer is the similarity between smooth and rough turbulent boundary layers. In a turbulent boundary layer, there are two flow regions identified, the inner and outer regions, and each region exhibits a distinct scaling. The similarity in the mean velocity in the outer layer can be assessed using velocity-defect scaling. Collapse of the mean defect profiles indicates that roughness effects on the mean flow are confined to the inner layer. On the other hand, lack of collapse indicates that roughness effects propagate into the outer region of the boundary layer (Connelly *et al.*, 2006).

There are three common choices for the outer velocity scale for the velocity defect profile in a turbulent boundary layer: the classical friction velocity, $u_\tau$; the freestream velocity, $U_e$, proposed by George and Castillo (1997); and ZS-scaling, $U_e \frac{\delta^*}{\delta}$, proposed by Zagarola and Smits (1998). In the following sections, these three parameters will be used to scale the mean velocity profiles in the form of the defect law in the context of both smooth- and rough-wall boundary layers. Based on the assumption of complete similarity, some theoretical derivations are used to further assess the effectiveness of the ZS-scaling.

## 4.2 Scaling of the Mean Velocity in Turbulent Boundary Layer

As described previously, the Log Law and defect law can be derived through some non-dimensional analysis. For the defect law, it assumes complete similarity in the outer region. This means if the appropriate outer velocity scale is chosen, all the mean velocity defect profiles scaled by it collapse onto a single curve, which implies that the effects of Reynolds number and roughness are eliminated.

As discussed previously, there are three common choices for the outer velocity scale for the velocity defect profile in the turbulent boundary layer: $u_\tau$, $U_e$ and $U_e \frac{\delta^*}{\delta}$. Traditionally, the same velocity scale in the inner region, $u_\tau$, has been used to scale the velocity defect profile in the outer region. Krogstadt and Antonia (1999) showed that the velocity defect profiles are similar for smooth and rough surfaces throughout the entire layer when scaled with $u_\tau$. Recently, based on their own similarity analysis, George and Castillo (1997) concluded that the outer velocity scale should be proportional to the freestream velocity, $U_e$. However, Bergstrom *et al.* (2002) used $U_e$ as the outer velocity scale for both smooth- and rough-wall boundary layers, and they found that the freestream velocity, $U_e$, was less effective than the friction velocity, $u_\tau$, as a scaling parameter for collapsing the defect profiles of different Reynolds numbers for the same surface.

Zagarola and Smits (1998) proposed a new outer velocity scale, $U_e \frac{\delta^*}{\delta}$, based on their study of turbulent pipe flows. This method has been successfully applied to the analysis of ZPG turbulent boundary layers, and it is commonly believed that the ZS-scaling represents the correct velocity scale for reproducing similarity in the form of the defect law. For example, Seo *et al.* (2004)

concluded that the ZS-scaling successfully removes the effects of different upstream conditions, Reynolds number and surface roughness from the outer flow for ZPG turbulent boundary layers. Zagarola and Smits (1998), Castillo and George (2001) and Akinlade *et al.* (2004), all indicated that the parameter, $\delta^*/\delta$, removes the effect of the upstream conditions on the outer velocity profile. Although the ZS-scaling has led to many successful results, its physical meaning is still lacking. According to Brzek *et al.* (2007), the ZS-scaling can be derived based on a similarity analysis which assumes a product of two functions. For example, assume that variable $G$ is the scaling factor which contains the effects of Reynolds number, $\delta^+$, roughness parameter, $k^+$, and upstream conditions, $\alpha$. As such, $G = G(\delta^+, k^+, \alpha)$. The outer similarity function, $\overline{f_o}$, is an asymptotic profile for ZPG flows. Then the non-dimensional velocity scaling law for the outer layer is expressed as

$$f_o(\bar{y}, \delta^+, k^+, \alpha) = G(\delta^+, k^+, \alpha)\overline{f_o}(\bar{y}) \qquad (4.1)$$

Substituting Eq. (4.1) into the definition of the displacement thickness, it follows that $G = \delta^*/\delta$, and $U_e \frac{\delta^*}{\delta}$ can be derived from the similarity analysis for rough surfaces.

## 4.3 Theoretical Analysis and Derivations

Zagarola and Smits (1998) proposed an outer velocity scale for the defect law based on their study of fully-developed pipe flows, and subsequently applied this new concept to the analysis of the wall boundary layer. The proposed velocity scale is $u_o = U_e \frac{\delta^*}{\delta}$. In the following analysis, a mathematical derivation will be used to examine the validity of this scale, which will then be used to investigate the similarity between smooth- and rough-wall boundary layers.

The following mathematical development is based on the assumption that complete similarity exists for boundary layers on a smooth surface and different kinds of rough surfaces. Owing to the assumed similarity, all of the scaled velocity profiles collapse onto a single curve, which implies that the area under the scaled velocity profiles must be equal to each other. The following analysis is inspired by but not the same as the theory of Weyburne (2008).

For the defect law, the area under the scaled profiles is given by:

$$\int_0^1 \frac{U_e - U}{u_o} d\left(\frac{y}{\delta}\right) = c_0 \qquad (4.2)$$

where $u_o$ is the outer velocity scale for complete similarity, $\delta$ is the outer length scale and $c_0$ is a nonzero constant which is equal to the dimensionless area under the curve.

After performing the integration of Eq. (4.2) from the wall ($y$ = 0) to the outer edge of the boundary layer edge ($y = \delta$), we obtain

$$c_0 = \frac{U_e \delta^*}{u_o \delta} \qquad (4.3)$$

where $\delta^* = \int_0^\delta \left(\frac{U_e - U}{U_e}\right) dy$ is the displacement thickness.

Then, the outer velocity scale, $u_o$, can be expressed as

$$u_o = \frac{U_e \delta^*}{\delta c_0} \qquad (4.4)$$

When $c_0$ is equal to 1, the outer scale proposed by Zagarola and Smits (1998) for the wall boundary layer is recovered, i.e., $u_o = U_e \frac{\delta^*}{\delta}$.

Recently, Weyburne (2008) stated that in order for similarity to hold in the 2-D wall boundary layer, the displacement thickness must be a similarity length scale. He also showed that the

velocity scaling variable must be proportional to the freestream velocity. From Eq. (4.4), it is clear that $u_o$ is proportional to the displacement thickness $\delta^*$ and the freestream velocity $U_e$. Weyburne (2008) also concluded that the ZS-scaling should be the perfect outer scale for different boundary layers.

Note that if we expect to obtain complete similarity across the entire boundary layer for two different flows, then for any location in the $y$ direction and not only the boundary layer edge, the area under the two velocity profiles must be equal. Therefore, $c_0$ should not be treated as a constant for the entire boundary layer, but instead is a function of $y/\delta$, and there are different values for $c_0$ for different $y$ locations. Based on this understanding, for any dimensionless location denoted by the variable $h$ $(= y/\delta)$ between 0 and 1, we obtain:

$$\int_0^h \frac{U_e - U}{u_o} d\left(\frac{y}{\delta}\right) = c_0(h) \qquad (4.5)$$

Here, we assume that $u_o$ is a constant for a specific flow, so that it can be moved to the right hand side of Eq. (4.5) to result in

$$\int_0^h (U_e - U)\, d\left(\frac{y}{\delta}\right) = c_0(h) \cdot u_o \qquad (4.6)$$

Furthermore, based on the conclusions of Weyburne (2008), we assume that $u_o$ is proportional to the freestream velocity $U_e$, the displacement thickness $\delta^*$ and a function of the boundary layer thickness $\delta$, i.e.,

$$u_0 = U_e \delta^* \cdot f(\delta) \qquad (4.7)$$

Note that when $f(\delta) = \frac{1}{\delta}$, $u_o$ becomes the outer scale proposed by Zagarola and Smits (1998).

Then substituting Eq. (4.7) into Eq. (4.6), we obtain:

$$\int_0^h \left(U_e - U\right) d\left(\frac{y}{\delta}\right) = c_0\left(h\right) \cdot U_e \delta^* \cdot f\left(\delta\right) \tag{4.8}$$

$$c_0\left(h\right) \cdot f\left(\delta\right) = \frac{\int_0^h \left(U_e - U\right) d\left(\frac{y}{\delta}\right)}{U_e \delta^*} \tag{4.9}$$

Any specific boundary layer will exhibit its own relationship based on $\delta$, $\delta^*$ and $U_e$. Note that $c_0(h)$ represents the dimensionless area under the defect profile from $y/\delta$ = 0 to the location $y/\delta = h$, and this quantity should be the same for flows which exhibit complete similarity.

If Eq. (4.9) is applied to descriptions of two different boundary layer flows, for flow 1,

$$c_0\left(h\right) \cdot f\left(\delta_1\right) = \frac{\int_0^h \left(U_{e1} - U_1\right) d\left(\frac{y}{\delta_1}\right)}{U_{e1} \delta_1^*} \tag{4.10 (a)}$$

and for flow 2,

$$c_0\left(h\right) \cdot f\left(\delta_2\right) = \frac{\int_0^h \left(U_{e2} - U_2\right) d\left(\frac{y}{\delta_2}\right)}{U_{e2} \delta_2^*} \tag{4.10 (b)}$$

If complete similarity holds between these flows, then the value of $c_0(h)$ is the same, and the ratio of the function $f(\delta)$ for the two flows is given by,

$$\frac{f\left(\delta_2\right)}{f\left(\delta_1\right)} = \frac{\frac{\int_0^h \left(U_{e2} - U_2\right) d\left(\frac{y}{\delta_2}\right)}{U_{e2} \delta_2^*}}{\frac{\int_0^h \left(U_{e1} - U_1\right) d\left(\frac{y}{\delta_1}\right)}{U_{e1} \delta_1^*}} \tag{4.11}$$

For the specific case of the ZS-scaling, the ratio of these functions is given by $\frac{f(\delta_2)}{f(\delta_1)} = \frac{\delta_1}{\delta_2}$. Furthermore, for complete similarity, the value of this ratio should be constant throughout the entire boundary layer.

In the next section, based on the analysis presented above, experimental data obtained from smooth- and rough-wall boundary layers in the wind tunnel will be used to assess the effectiveness of the ZS-scaling and determine if complete similarity holds between two boundary layer flows.

## 4.4 Results and Discussions

Figure 4.1 compares the mean velocity profiles for the smooth and rough surfaces using inner coordinates based on the experimental data of Akinlade (2005). As expected, the effect of surface roughness is to increase the friction velocity, which further results in a downward shift of the mean velocity profiles referred to as the roughness shift, $\Delta U^+$. By definition, $\Delta U^+$ is zero for a smooth surface. As indicated previously in Table 3.1, the rough surface exhibits a stronger wake component than does the smooth surface.

Figure 4.2 presents the mean velocity defect profiles for the smooth and rough surfaces, where the friction velocity, $u_\tau$, the freestream velocity, $U_e$ and ZS-scaling, $U_e \frac{\delta^*}{\delta}$ are used to scale the velocity profiles, respectively, and the boundary layer thickness, $\delta$, is used as the outer length scale. By comparing these three profiles, it is apparent that the friction velocity and ZS-scaling

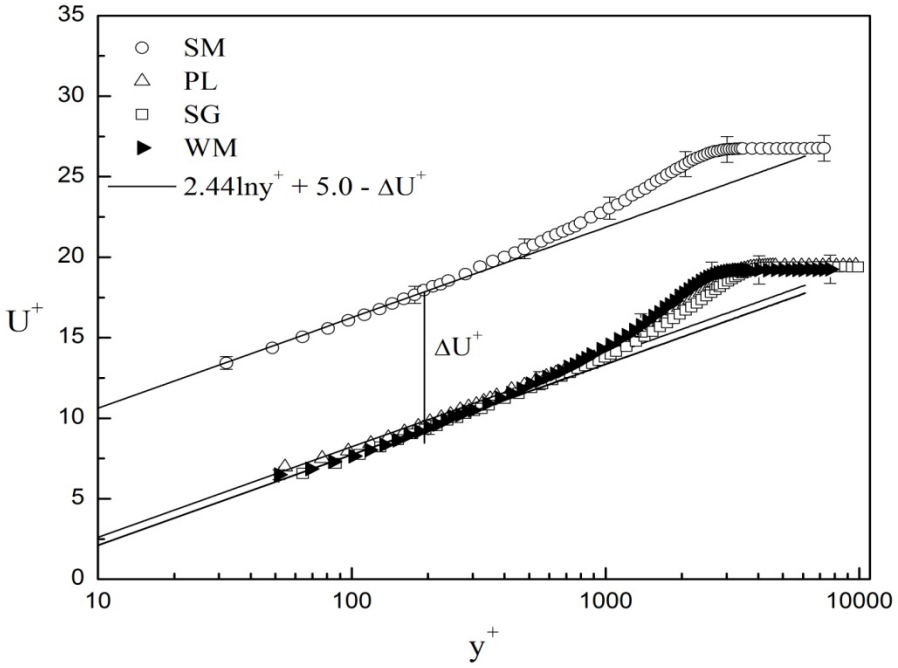


Figure 4.1: Mean velocity profiles for smooth and rough walls displayed using inner coordinates.

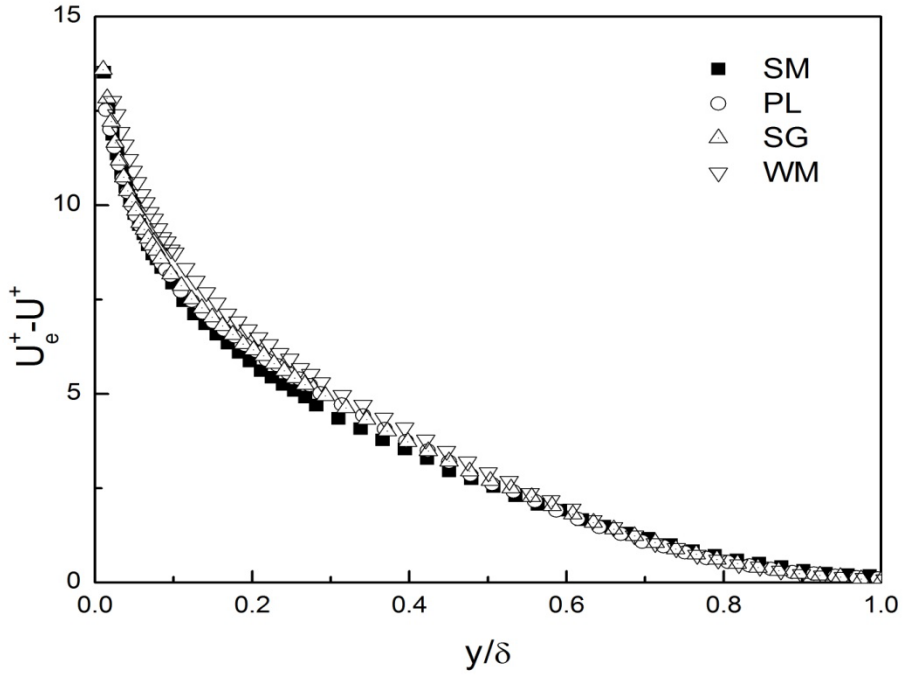


a)

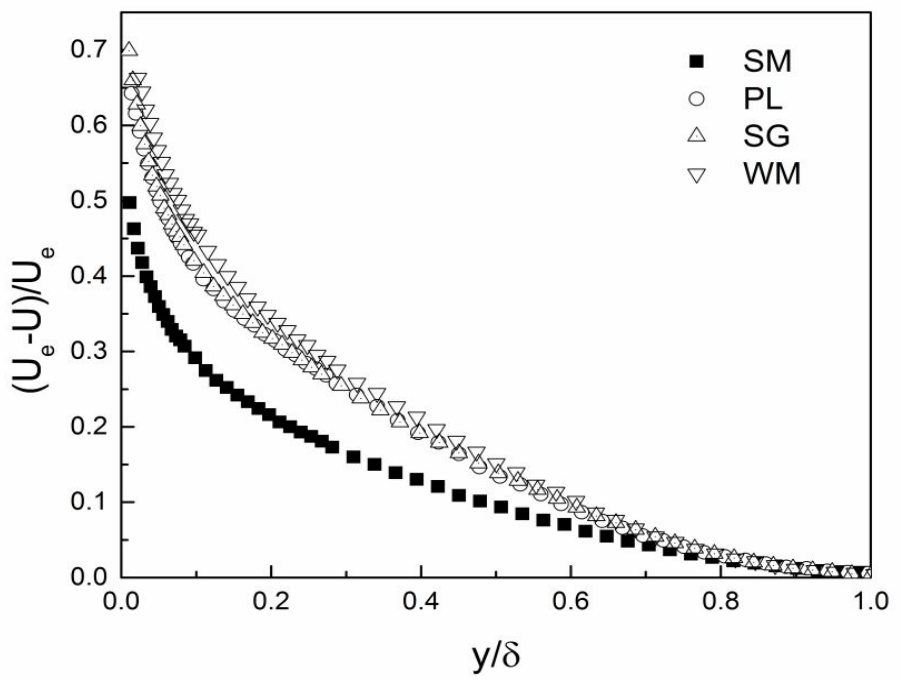


b)

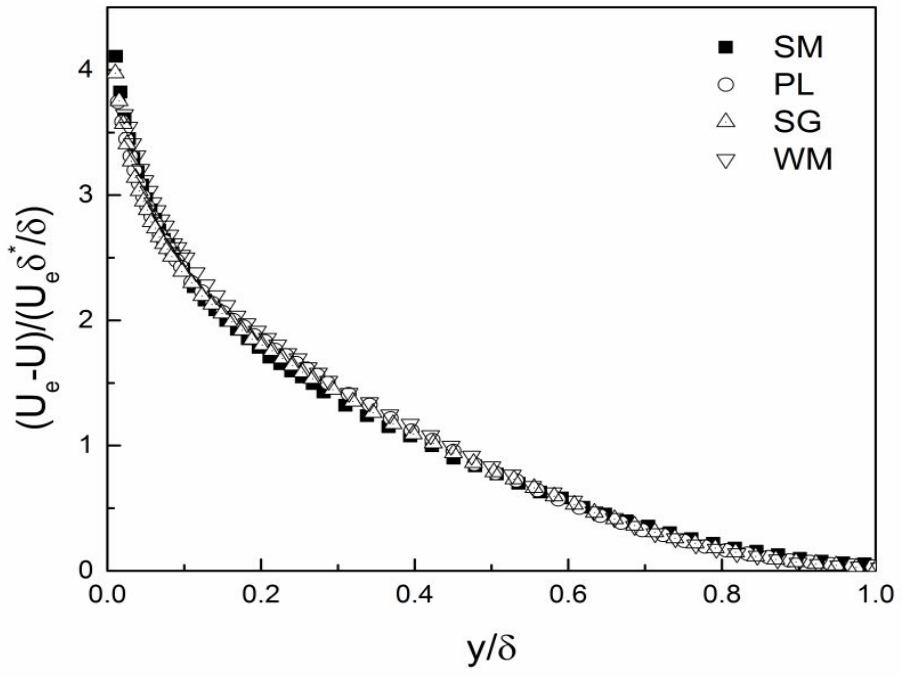


c)

Figure 4.2: Mean velocity defect profiles scaled by: a) $u_\tau$; b) $U_e$; c) $U_e \frac{\delta^*}{\delta}$.

are more effective than $U_e$ for collapsing the mean velocity defect profiles. Both the friction velocity and ZS-scaling give similar performance in the entire boundary layer.

As presented in Figure 4.3, the defect profiles are also displayed using semi-logarithmic coordinates for the more critical assessment of the agreement between velocity defect profiles in the overlap and outer regions. Clearly, the mean velocity defect profiles do not collapse when scaled by $U_e$. On the other hand, the defect profiles scaled by $u_\tau$ and ZS-scaling collapse onto a single curve in the outer region from $y = 0.1\delta$ to $y = \delta$. It also appears that the ZS-scaling performs somewhat better than $u_\tau$ in the inner region. Overall, the results here confirm well the widely accepted conclusion that ZS-scaling is an effective scale for the mean velocity defect law in the outer region (Brzek *et al.* (2007); Seo *et al.* (2004); Akinlade *et al.* (2004)). However, note that the velocity profiles of WM behave differently from the other two kinds of rough surfaces in the range of $y/\delta = 0.01$ to $y/\delta = 0.1$. The reason for this difference may be that WM is a very distinct type of roughness with elements elevated above the ground plane. As shown in Figure 4.1, although the velocity profile of WM has been modified by changing the values of the friction velocity, $u_\tau$ and the virtual origin, $y_0$, it still has slightly different behaviors of being parallel to the Log Law as the other rough surfaces. Therefore, the original data of WM may have slightly larger errors than the others. However, the trend of the velocity profiles of WM is consistent with the others, and the slight difference observed here does not alter our conclusions.

Figure 4.4 compares the ratios obtained using Eq. (4.11) for different pairs of surfaces based on the experimental data and also calculated from the theory of ZS-scaling. As discussed in the previous section, this ratio is derived based on the assumption of the complete similarity in the entire boundary layer. Furthermore, the experimental results can be compared to the curves

corresponding to the theory proposed by Zagarola and Smits (1998) to assess the effectiveness of the ZS-scaling for the defect law.

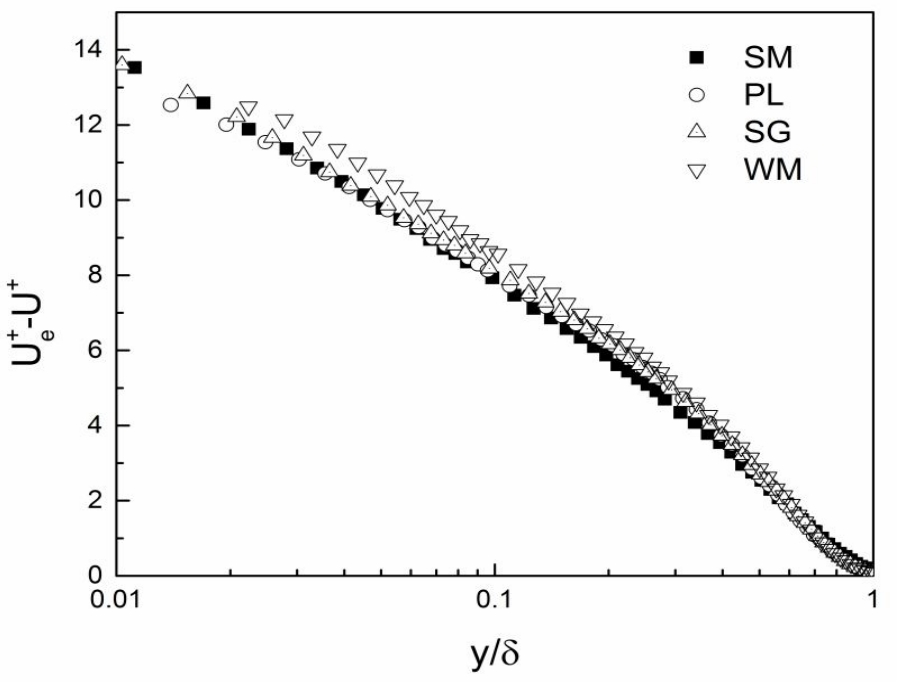


a)

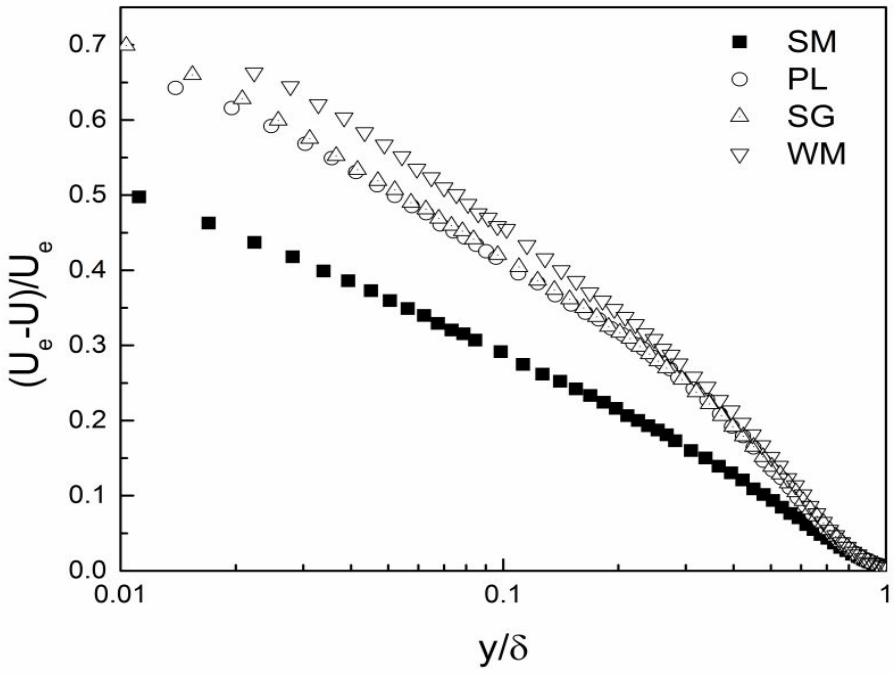


b)

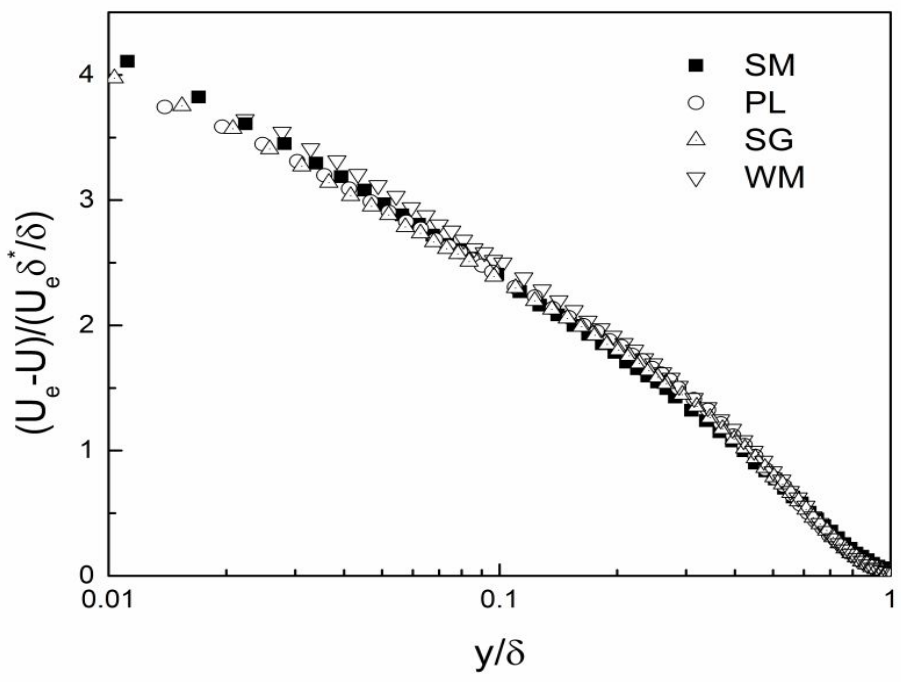


c)

Figure 4.3: Mean velocity defect profiles scaled in the semi-logarithmic coordinates by: a) $u_\tau$; b) $U_e$; c) $U_e \frac{\delta^*}{\delta}$.

Table 4.1 presents the values of Eq. (4.11) based on the ZS-scaling for different types of flows. Recall that for the ZS-scaling, $\frac{f(\delta_2)}{f(\delta_1)} = \frac{\delta_1}{\delta_2}$, and it is expected to be constant over the entire boundary layer. In Figure 4.4, horizontal lines corresponding to these constant values are plotted and compared with the experimental results.

Table 4.1: Constant values of the ratio in Eq. (4.11) based on the ZS-scaling.

| | PL/SM | SG/SM | WM/SM | PL/SG | PL/WM | SG/WM |
|---|---|---|---|---|---|---|
| $f(\delta_2)/f(\delta_1)$ | 1.0544 | 1.0576 | 0.9815 | 0.9969 | 1.0744 | 1.0777 |

As is clear in Figure 4.4, the curves based on the experimental data are not horizontal. They can be classified into two groups, each group with three curves. The first group represents the ratios between a pair of different types of rough surfaces, while the second group represents the ratios between a smooth and a rough surface. As shown in the figure, for the first group, the curves are approximately horizontal over the entire boundary layer, whereas for the second group, the curves are not horizontal in the region from $y = 0$ to $y = 0.4\delta$, but trend towards a horizontal pattern after $y = 0.4\delta$.

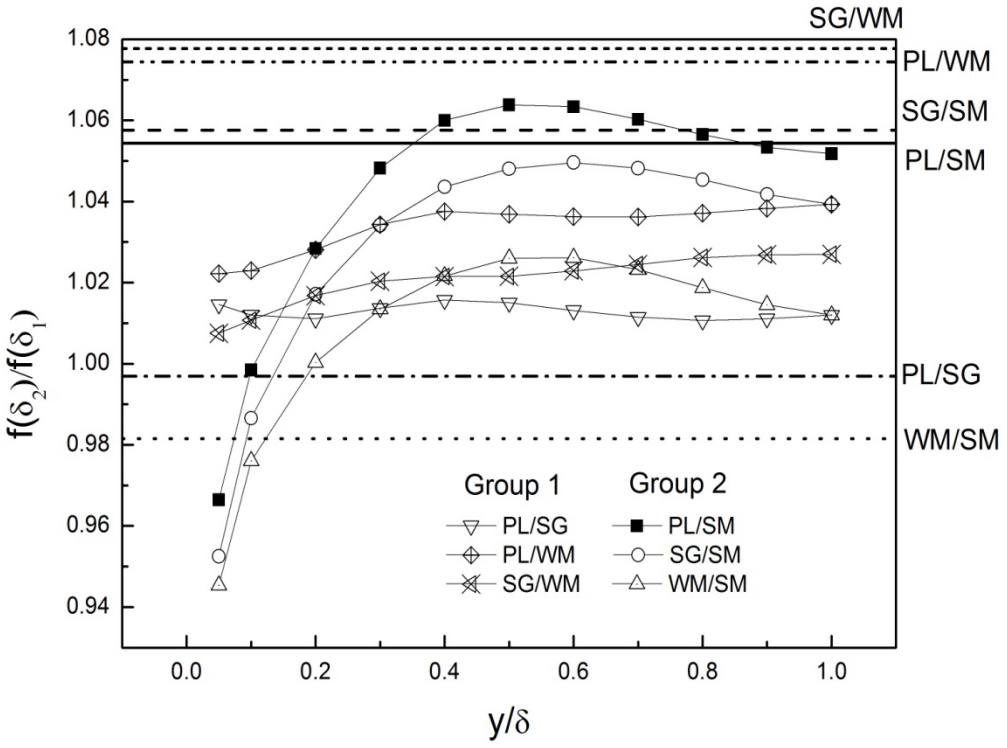


Figure 4.4: Comparisons of the ratios calculated from Eq. (4.11) between different types of surfaces based on the experimental data and ZS-scaling.

By comparing the horizontal parts of the experimental curves with the constants based on the ZS-scaling, it is observed that their differences are all under 5 %. Based on the experimental uncertainty, these differences are likely not significant. This suggests that the ZS-scaling is an

effective velocity scale for describing similarity between different types of rough-wall boundary layers (group 1) and similarity between the smooth- and rough-wall boundary layers (group 2), but only in the region from $y = 0.4\delta$ to $y = \delta$. This conclusion is consistent with the previous assessments of Bergstrom *et al.* (2002) and Akinlade *et al.* (2004). Furthermore, this analysis suggests that the ZS-scaling is not an appropriate velocity scale for achieving similarity between smooth- and rough-wall boundary layers in the region from $y = 0$ to $y = 0.4\delta$ (which includes the inner layer, the overlap region and part of the outer region). These results also indicate that the degree of the collapse between different mean velocity profiles is much less for the inner region and part of the outer region. This challenges the widely accepted idea that ZS-scaling is an effective scale for the mean velocity defect law throughout the outer region.

Furthermore, based on the approach of Connelly *et al.* (2006), the similarity of different boundary layers can be assessed by using the scaled mean velocity profiles in the form of the defect law. The different behaviors observed for the smooth and rough surfaces in the region from $y = 0$ to $y = 0.4\delta$, imply that the boundary layers developed over the smooth and rough surfaces do not exhibit similarity in this region, and the effects of roughness elements extend into the outer region and are not confined to the inner layer. This is similar to the conclusions of Krogstad *et al.* (1992), Tachie *et al.* (2000) and Akinlade *et al.* (2004) that the velocity profiles for the different surfaces are distinct from each other not only in the wall region but also over a significant part of the outer region of the boundary layer. In addition, based on the similar behavior of the ratios for different rough surfaces across the entire boundary layer, one can conclude that for different fully rough surfaces, complete similarity holds over the entire turbulent boundary layer, and different kinds of roughness elements produce the same effects on the mean velocity structure of the turbulent boundary layers.

Figure 4.5 compares the ratios calculated using Eq. (4.11) for different freestream velocities. These curves are based on mean velocity measurements obtained in a wind tunnel as described in Chapter 3. Similar to Figure 4.4, the curves represent the results from the experimental data, and the theoretical results based on the ZS-scaling are in the form of horizontal lines. Boundary layer profiles for two freestream velocities ($U_e$ = 30 m/s and 40 m/s) were both measured on the smooth surface. In Figure 4.5, numbers "30" and "40" indicate the values of freestream velocities, and letters "S" and "R" refer to the smooth surface and a fully rough surface made of 40-d grit sandpapers, respectively. For this data set, the ratios between the smooth and rough surfaces exhibit the same behavior as shown in Figure 4.4, which confirms that the previous conclusions hold for different Reynolds numbers. For the results for different freestream velocities on the smooth surface, the theoretical values obtained from ZS-scaling agree well with those obtained from the experimental data, which further confirms that the ZS-scaling can eliminate the effects of Reynolds numbers.

Note that for the plot of 30S/40S, the part in the inner region is not as horizontal as expected. The reason for this difference may be due to the error of the origin of $y$ location. The results in the inner region are very sensitive to the first measured location in $y$ direction, such that the profile may not behave as expected. However, the overall trend maintains horizontal, and the results presented here in general support the conclusions addressed in the previous paragraph.

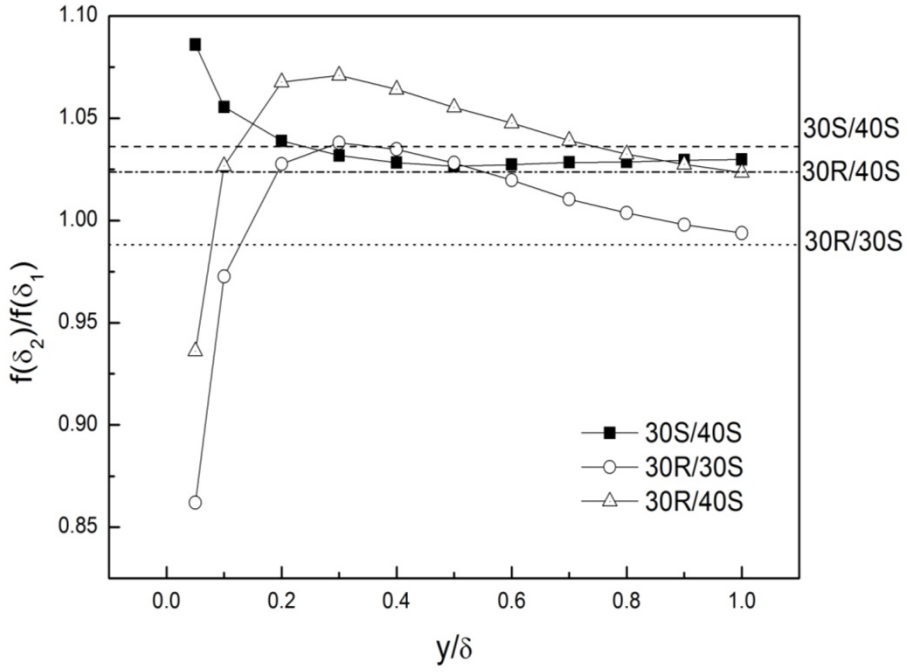


Figure 4.5: Comparison of ratios calculated using Eq. (4.11) for different Reynolds numbers.

## 4.5 Summary

In this chapter, a mathematical equation is formulated to assess the assumption of complete similarity between turbulent boundary layers on different types of rough and smooth surfaces. A ratio of a scaling function is used to assess the ZS-scaling method (Zagarola and Smits, 1998) on describing the similarity between different kinds of turbulent boundary layers. By comparing the results from wind tunnel experiments on smooth and rough surfaces with the theory of Zagarola and Smits (1998), the following conclusions can be obtained:

(1) Comparisons of the mean velocity defect profiles scaled by the friction velocity, $u_\tau$, the freestream velocity, $U_e$ and ZS-scaling, $U_e \frac{\delta^*}{\delta}$ in both regular and semi-logarithmic

coordinates confirm the viewpoint that the ZS-scaling is the most effective outer scale for the mean velocity profiles. The ZS-scaling outperforms the velocity scales represented by $u_\tau$ and $U_e$, and is able to successfully integrated the roughness effects.

(2) Using the ratio of scaling functions (derived based on the assumption of complete similarity in the entire boundary layer), the experimental and ZS-scaling results are compared. It is concluded that the ZS-scaling is an effective mean velocity scale for assessing similarity between different types of rough surfaces over the entire turbulent boundary layer, as well as similarity between smooth and rough surfaces in the outer region. However, the ZS-scaling is much less effective in the region from $y = 0$ to $y = 0.4\delta$, which includes the inner layer, the overlap region and part of the outer region. This conclusion challenges the widely accepted viewpoint that the ZS-scaling is an appropriate scale for the mean velocity defect profile in both the overlap and outer regions. The results from different Reynolds numbers further confirm that the ZS-scaling is insensitive to the Reynolds number when it is used for describing the similarity of turbulent boundary layers.

(3) The discrepancies in ratio of scaling functions for the smooth and rough surfaces in the region from $y = 0$ to $y = 0.4\delta$ suggests that similarity does not exist in this region and the effects of the roughness extend into the outer region and are not confined just to the inner layer. Furthermore, the fact that the ratios between different types of rough surfaces exhibit similar behavior indicates that for fully rough surfaces, the roughness elements of different geometries have the similar effects on the structure of the turbulent boundary layer.

# 5 CHARACTERISTICS OF FLOW OVER A STEP CHANGE IN ROUGHNESS

## 5.1 Introduction

How a turbulent boundary layer develops over a step change in roughness is in another important topic, which has vast applications in both engineering and meteorology. A major feature of turbulent flow over a step change in roughness is the generation of an IBL. The IBL is commonly considered to be the region where the flow is influenced by the new surface condition. In this chapter, the flow over a smooth-rough-smooth transition is investigated experimentally in a wind tunnel based on velocity measurements using a boundary layer Pitot tube. Mean velocity profiles at different $x$ direction (streamwise) locations are obtained. The results indicate that the flow in the inner layer is immediately affected by the new surface condition due to the change in skin friction, and the roughness effects propagate in the wall-normal direction as the IBL grows in the streamwise direction. In order to study this propagation effects, the development of the IBL thickness, $\delta_i$, in the $x$ direction was assessed using the method of Antonia and Luxton (1971, 1972).

## 5.2 Mean Velocity Profiles

Figure 5.1 presents the mean velocity profiles at different $x$ locations over the smooth-rough and rough-smooth transitions for different freestream velocities, i.e., $U_e$ = 20 m/s, 30 m/s and 40 m/s.

The results clearly illustrate the development of the flow passing over the two step changes in roughness. In general, similar behavior is observed for all three freestream velocities.

Figure 5.1 a), c) and e) show the development of the flow over the smooth-rough transition at three freestream velocities. When the flow encounters the rough surface, the fluid in the inner layer is immediately decelerated due to the enhanced skin friction associated with the surface roughness. However, the fluid in the outer layer ($y$ = 3-10 mm, and approximately $y^+$ = 300-1000) is not initially affected by the surface roughness, as such the mean velocity profiles in this region and above are almost identical to those on the smooth surface. With the increasing distance in the $x$ direction, the roughness effects propagate further into the flow, and the profiles in both the inner and outer layers gradually depart from that of the smooth surface. When the flow reaches the last measurement streamwise location on the rough surface ($x_1$ = 200 mm), the profile becomes almost identical to that at the previous location ($x_1$ = 160 mm). This suggests that the flow may have completely adjusted to the new condition of the rough surface, and any further measurement is not needed on the rough surface after $x_1$ = 200 mm.

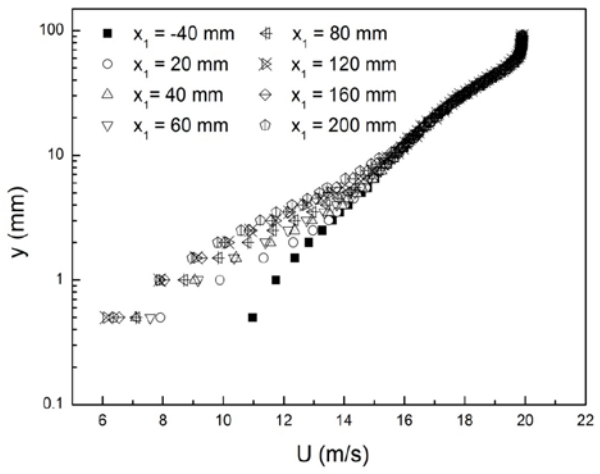


a)

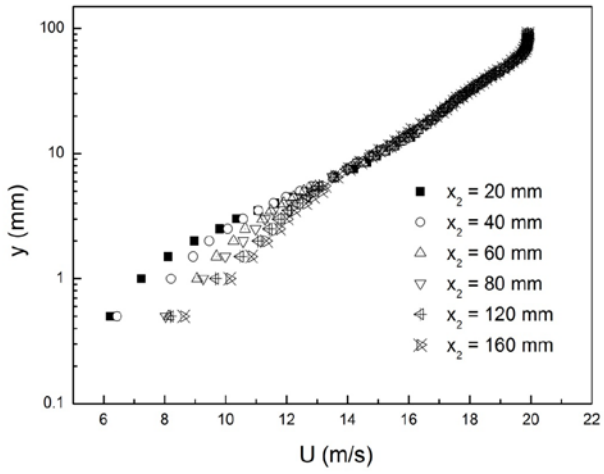


b)

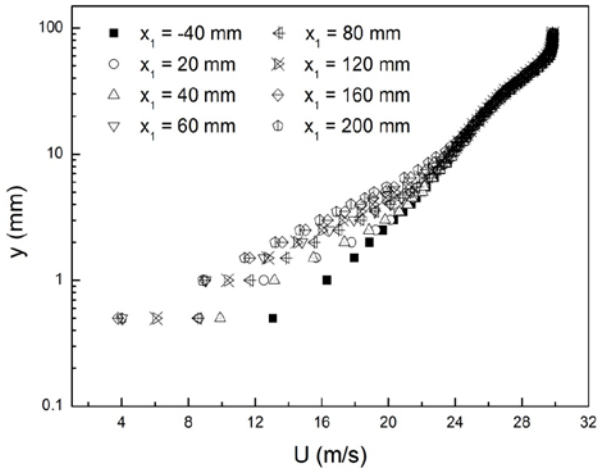


c)

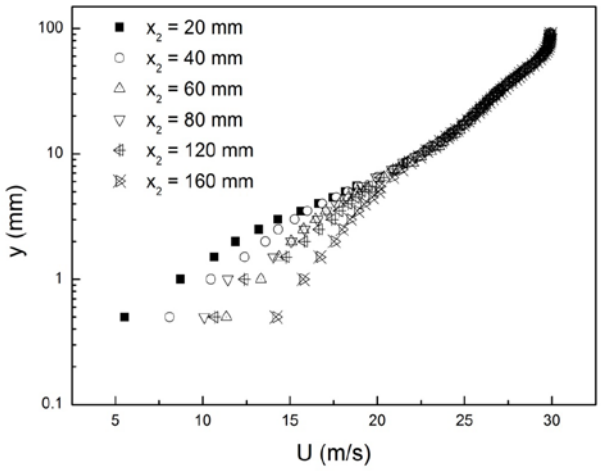


d)

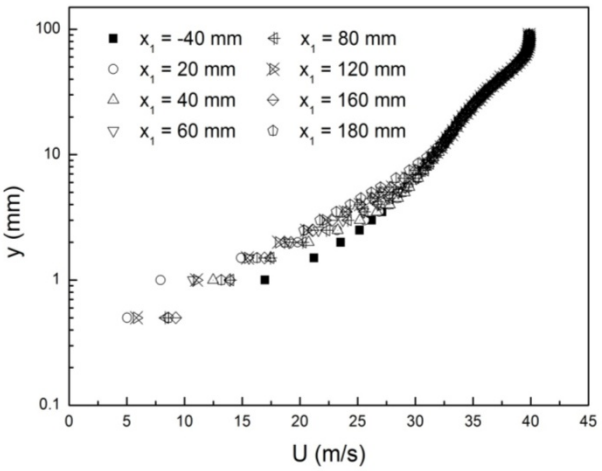


e)

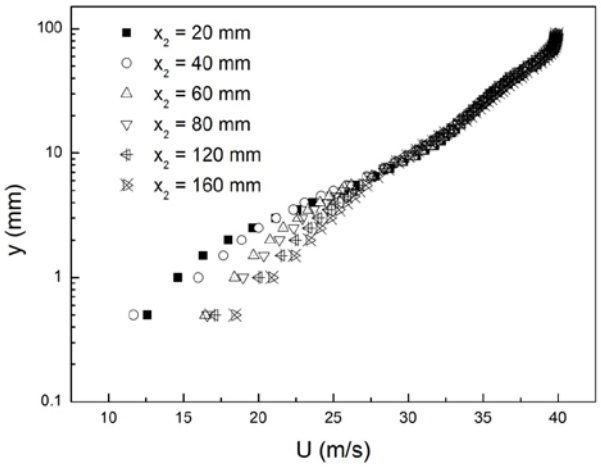


f)

Figure 5.1: Mean velocity profiles over smooth-rough-smooth transition for different freestream velocities. a) Smooth-rough for $U_e$= 20 m/s; b) Rough-smooth for $U_e$= 20 m/s; c) Smooth-rough for $U_e$= 30 m/s; d) Rough-smooth for $U_e$= 30 m/s; e) Smooth-rough for $U_e$= 40 m/s; f) Rough-smooth for $U_e$= 40 m/s.

Figure 5.1 b), d) and f) show how the flow develops when the surface condition changes back to the smooth case. The process is the reverse scenario to the smooth-rough transition. The fluid in the inner layer is initially influenced by the new surface condition, and the effects of the smooth surface gradually propagate into the flow. Unlike the smooth-rough transition, at the last

measured location ($x_2$ = 160 mm), there is no collapse of the velocity profiles. This implies that the influence of the smooth surface continues to penetrate further into the flow at this location, and the growth rate of the IBL over a rough-smooth transition is lower than that over a smooth-rough transition. This can be physically explained by the fact that the smooth surface creates less skin friction than the rough surface.

To further illustrate the flow development over the step change in roughness, some select data over the entire smooth-rough-smooth transition region are plotted in inner coordinates for different freestream velocities in Figure 5.2. Here, inner coordinates uses the dimensionless velocity $u^+ = \frac{U}{u_\tau}$ and wall-normal distance $y^+ = \frac{yu_\tau}{\nu}$. The friction velocity, $u_\tau$, is obtained by fitting the mean velocity profile on the smooth surface at the location $x_1$ = -80 mm to the Log Law. The results show a similar flow development process as in Figure 5.1. Note that the velocity profile at the last measured location on the second smooth surface exhibits a different behavior than that on the first smooth surface, and any recovery to the Log Law is incomplete. This also implies that parts of the velocity profile may preserve an “immediate memory” of the previous surface condition, and therefore are not in equilibrium with the local surface.

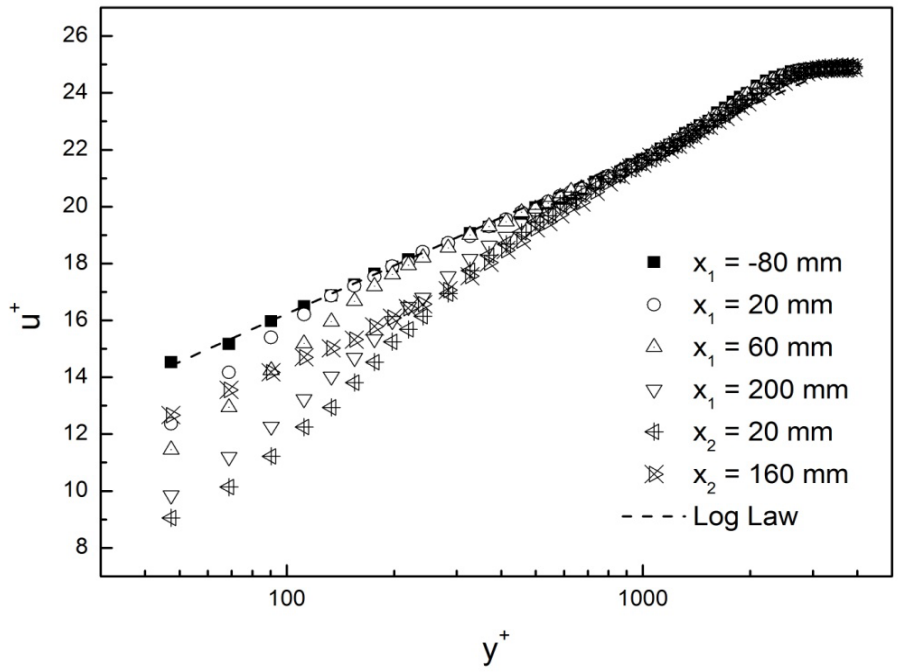
26
24
22
20
18
16
14
12
10
8
u+
100
1000
y+
x1 = -80 mm
x1 = 20 mm
x1 = 60 mm
x1 = 200 mm
x2 = 20 mm
x2 = 160 mm
Log Law

a)

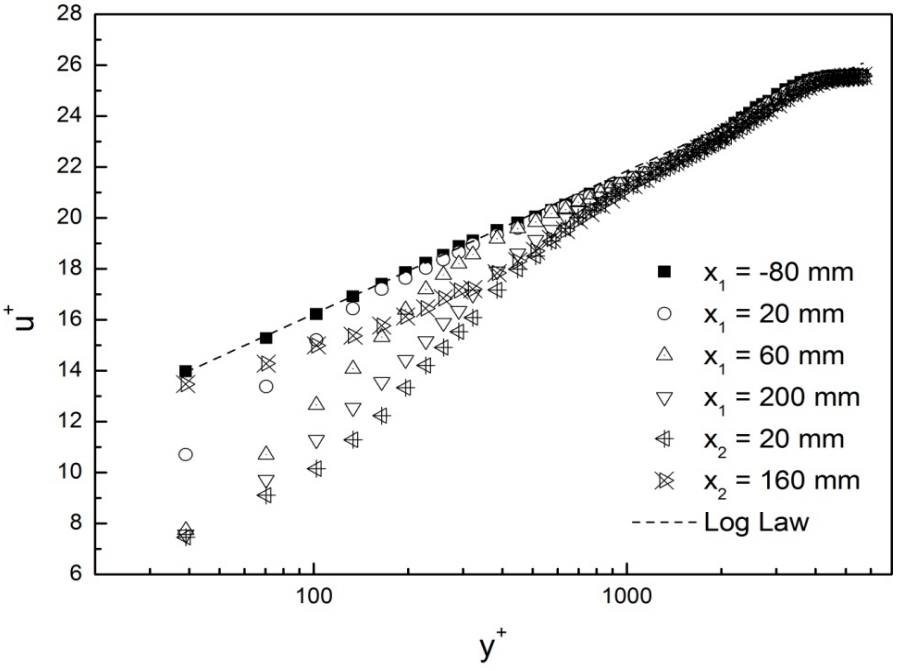
28
26
24
22
20
18
16
14
12
10
8
6
u+
100
1000
y+
x1 = -80 mm
x1 = 20 mm
x1 = 60 mm
x1 = 200 mm
x2 = 20 mm
x2 = 160 mm
Log Law

b)

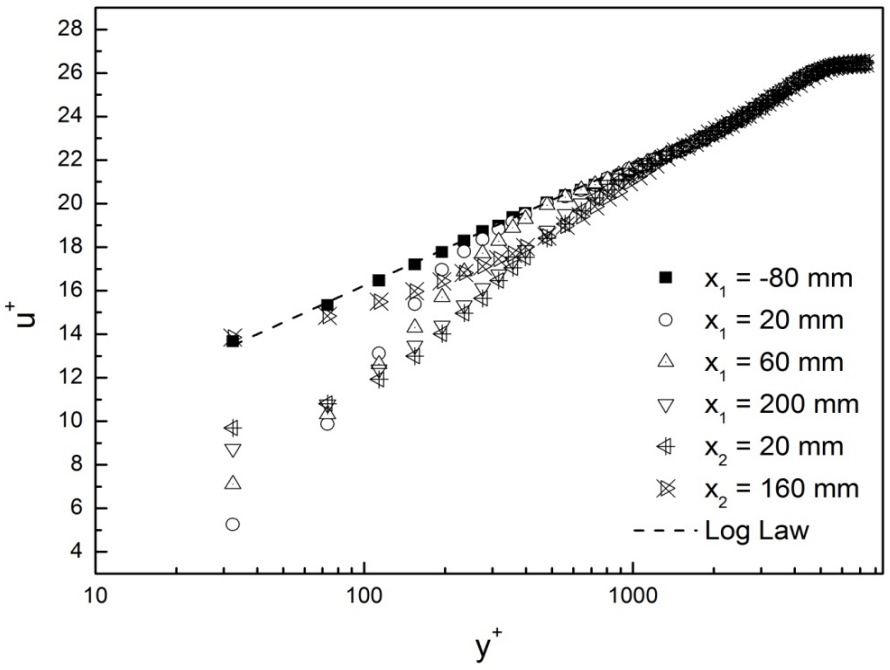


c)

Figure 5.2: Select mean velocity profiles over the smooth-rough-smooth surface change in the inner coordinates for different freestream velocities. a) $U_e$= 20 m/s; b) $U_e$= 30 m/s; c) $U_e$= 40 m/s.

## 5.3 Boundary Layer Thicknesses

Figure 5.3 demonstrates the streamwise developments of the displacement and momentum boundary layer thicknesses and shape factor. As indicated in Figure 5.3 a), the displacement thickness, $\delta^*$, keeps growing after the change from the smooth to rough surface for all three different freestream velocities. In contrast, the profiles become different after the change from the rough to smooth surface. By definition, $\delta^*$ is the distance by which the upper streamline of a viscous fluid (of freestream velocity $U_e$) needs to be displaced vertically off the wall in order topreserve the same mass flow rate as in the case when fluid viscosity is absent. After the first

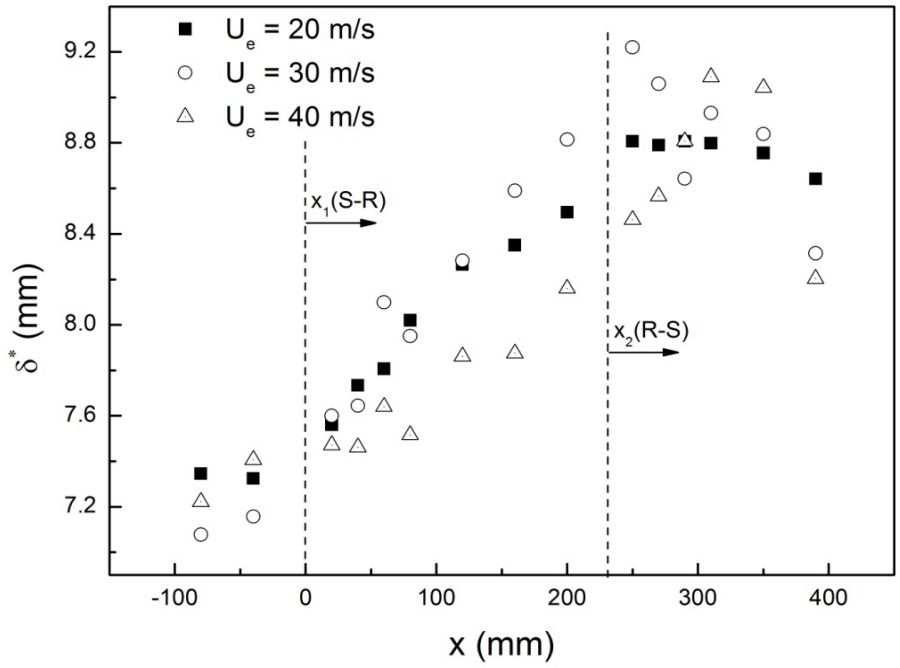
U_e = 20 m/s
U_e = 30 m/s
U_e = 40 m/s
x_1(S-R)
x_2(R-S)
δ* (mm)
x (mm)
9.2
8.8
8.4
8.0
7.6
7.2
-100
0
100
200
300
400

a)

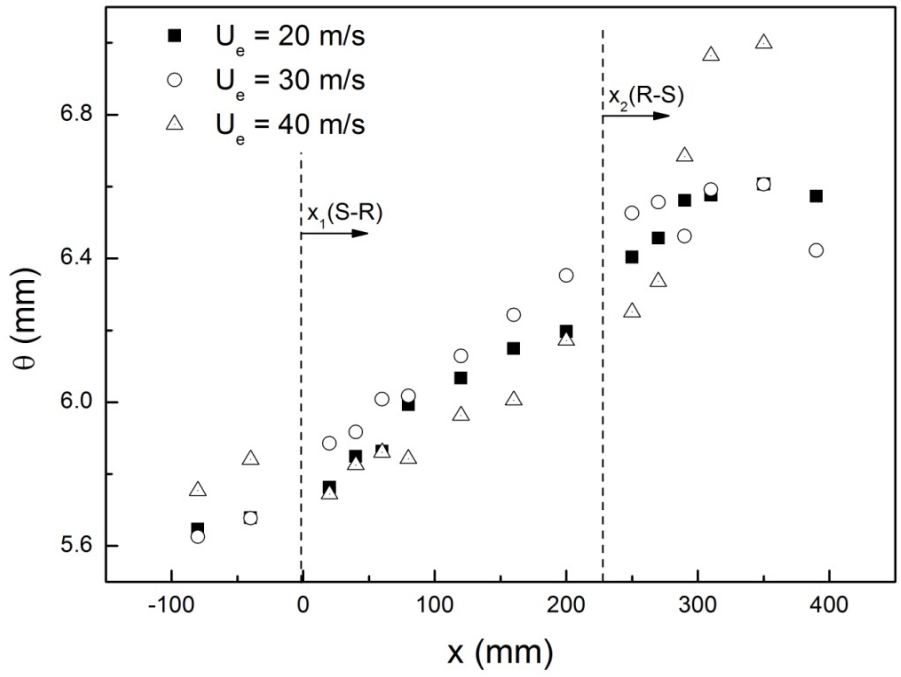
U_e = 20 m/s
U_e = 30 m/s
U_e = 40 m/s
x_1(S-R)
x_2(R-S)
θ (mm)
x (mm)
6.8
6.4
6.0
5.6
-100
0
100
200
300
400

b)

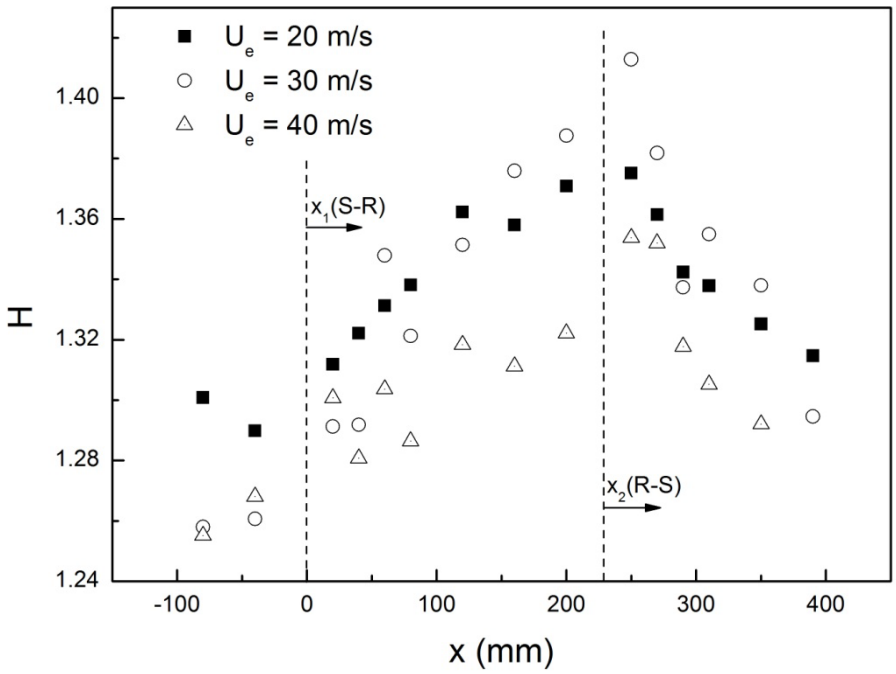


c)

Figure 5.3: Streamwise development of the displacement and momentum thicknesses of the smooth-rough-smooth boundary layer: a) Displacement thickness, $\delta^*$; b) Momentum thickness, $\theta$; and c) Shape factor, $H$.

in surface condition (starting from $x_1$ = 0) the effect of roughness is to increase the value of $\delta^*$, however after the second change in surface condition (starting from $x_2$ = 0) the smooth surface tends to decrease the value of $\delta^*$.

In addition, the development of the momentum thickness is indicated in Figure 5.3 b). by definition, the momentum thickness, $\theta$ ($= \int_0^{\delta} \frac{U}{U_e}\left(\frac{U_e - U}{U_e}\right) dy$ ), is the local momentum deficit carried by the local mass flux, and this quantity is related to the drag caused by the boundary layer.

The shape factor, $H = \delta^*/\theta$, plotted in Figure 5.3 c), in general increases after the smooth-rough transiton and decreases after the rough-smooth transition. This phenomenon is consistent with the characteristics of the shape factor, i.e., it has a larger value on a rough surface and a smaller value on a smooth surface, and $H$ decreases with the Reynolds number.

## 5.4 Determination of Internal Boundary Layer Thickness $\delta_i$

As mentioned in Chapter 2, the definition of an IBL is somewhat unclear, and there are multiple methods to determine the IBL thickness $\delta_i$. In this section, the method proposed by Antonia and Luxton (1971, 1972) is used to determine the IBL thickness. In their research, Antonia and Luxton (1971, 1972) observed that the mean velocity profiles inside the internal layer in the region near the surface exhibited a linear trend when plotted in the form $U$ vs. $y^{1/2}$. It was also found that the mean velocity distribution outside the internal layer could be conveniently plotted in the same coordinates, which exhibits a different linear trend except for the region very close to the outer edge of the boundary layer. In view of this, for the specific case of our smooth-rough-smooth boundary layer flow, it is expected that there exists an intersection of the two straight lines (which reflect the two different linear behaviours) close to the edge of the IBL. In the following context, the method of Antonia and Luxton (1971, 1972) is used to determine the IBL thickness and to investigate the development of IBLs after the roughness changes.

Figure 5.4 compares the mean velocity profiles plotted using $U/U_e$ vs. $y^{1/2}$ coordinates for the three freestream velocities tested. The results show the development of the flow after two roughness changes. As expected, two straight lines are clearly evident in the inner and outer

regions. The intersections of these straight lines can be applied to determination of the IBL thickness.

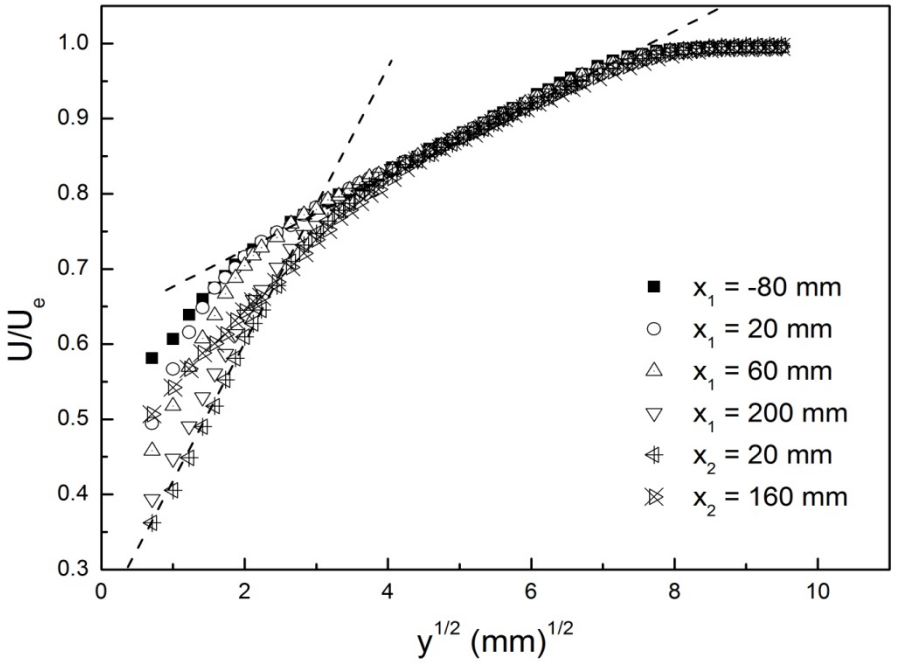


a)

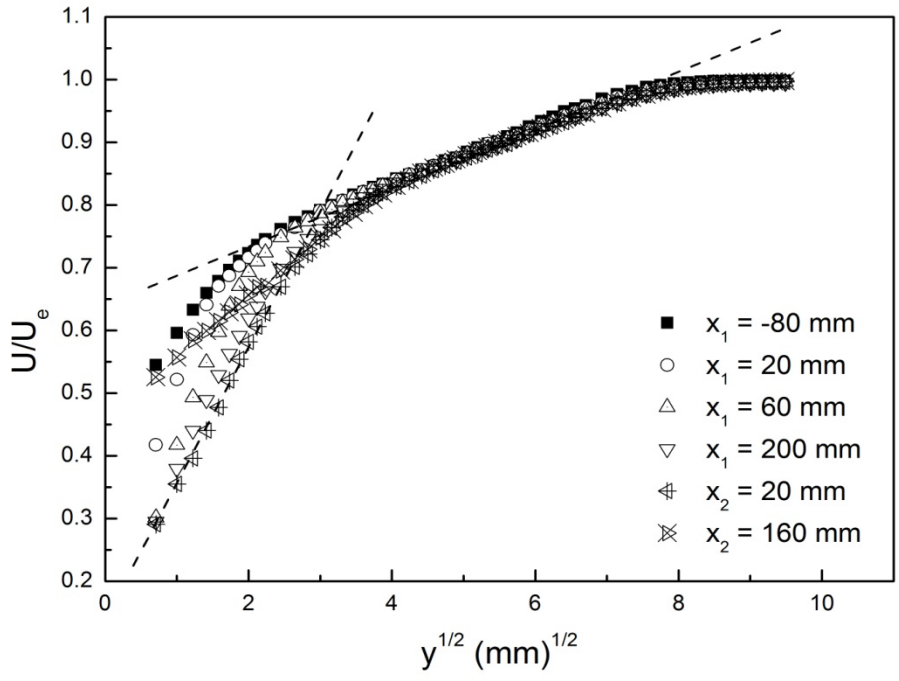


b)

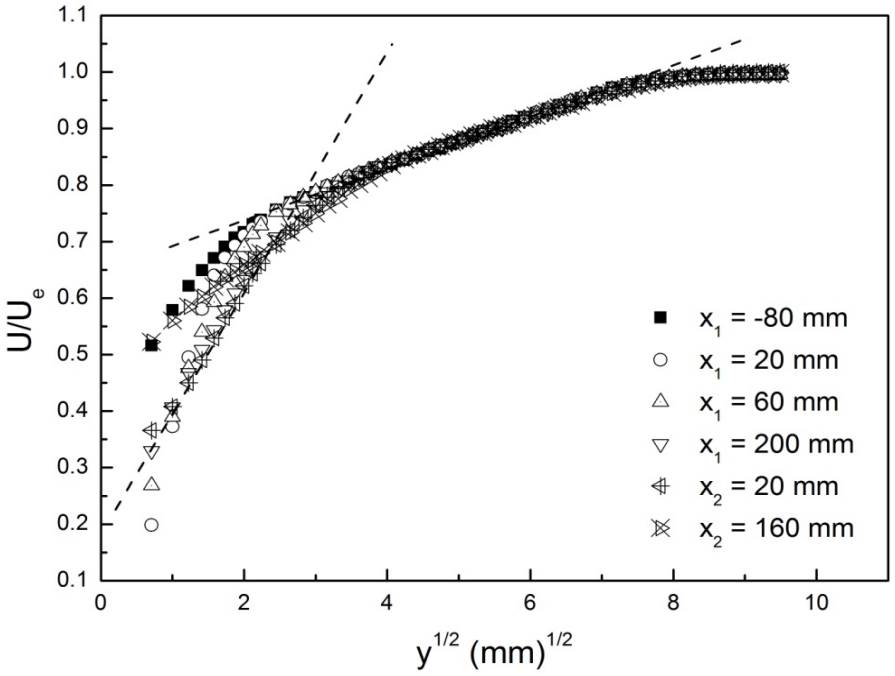


c)

Figure 5.4: Comparisons of the mean velocity profiles plotted using $U/U_e$ vs. $y^{1/2}$ coordinates at different streamwise locations: a) $U_e$ = 20 m/s.; b) $U_e$ = 30 m/s; c) $U_e$ = 40 m/s.

In order to refine the study, Figure 5.5 demonstrates two examples on how to determine the IBL thickness using the method of Antonia and Luxton (1971, 1972). The "knee" point, i.e., the intersection of the straight lines on the half-power plot $U/U_e$ vs. $y^{1/2}$ can be used to determine the value of $(\delta_i)^{1/2}$, accordingly, the IBL thickness, $\delta_i$ can be conveniently obtained. From Figure 5.5, the IBL thicknesses for the two selected cases are $\delta_i$ = 4.1250 mm for $U_e$ = 30 m/s and $x_1$ = 60 mm, and $\delta_i$ = 11.4001 mm for $U_e$ = 30 m/s and $x_2$ = 60 mm. In the next section, the study on IBL thickness will be further refined. The value of $\delta_i$ for all locations in the $x$ direction will be determined. As such, the growth rate of $\delta_i$ along the $x$ direction will be quantified for further analysis of the characteristics of the flow over the step change in roughness.

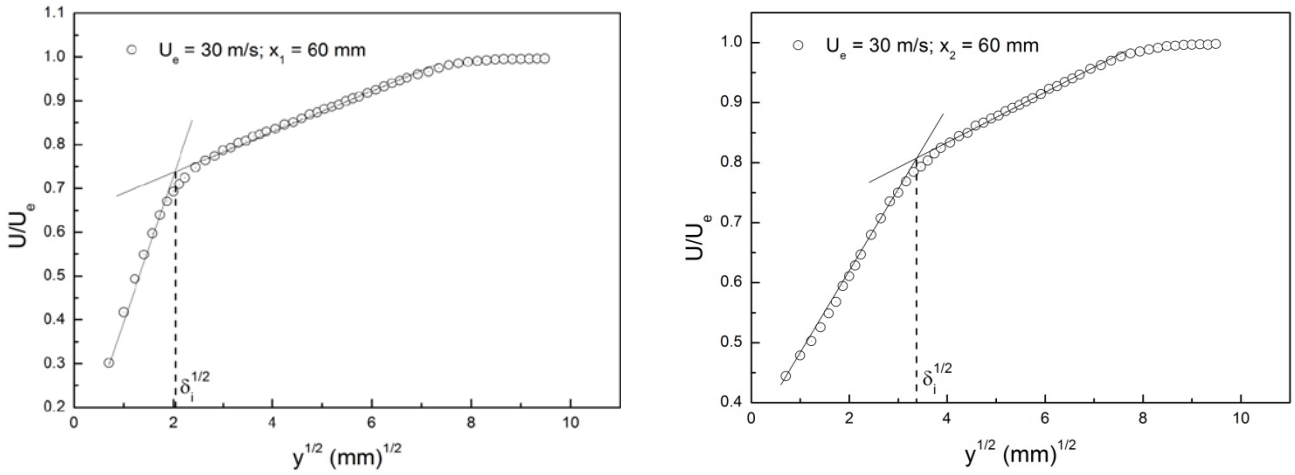


a) b)

Figure 5.5: Examples on using the method of Antonia and Luxton to determine the IBL thickness: a) $U_e$ = 30 m/s, $x_1$ = 60 mm (on the rough surface); b) $U_e$ = 30 m/s, $x_2$ = 60 mm (on the second smooth surface).

## 5.5 Growth Rate of Internal Boundary Layer Thickness

Based on the method of Antonia and Luxton (1971, 1972), the growth rate of the IBL thickness, $\delta_i$, is plotted in Figure 5.6. Figures 5.6 a), b) and c) demonstrate the growth rates of $\delta_i$ for three different freestream velocities, and in each case, curves are fitted to the results. In Figures 5.6 a), b) and c), the streamwise growth rates of the IBL thickness are given by empirical equation through curve fitting to the power relation using the software Excel. The exponents of these equations are very close for either smooth-rough or rough-smooth transition. For further comparison and analysis, the results for all three freestream velocities are plotted together in Figure 5.7, which shows that the growth rates for these three different conditions are similar for both the smooth-rough and rough-smooth transitions. In view of this, it can be concluded that the

Reynolds number based on the freestream velocity has little influence on the development of the IBL.

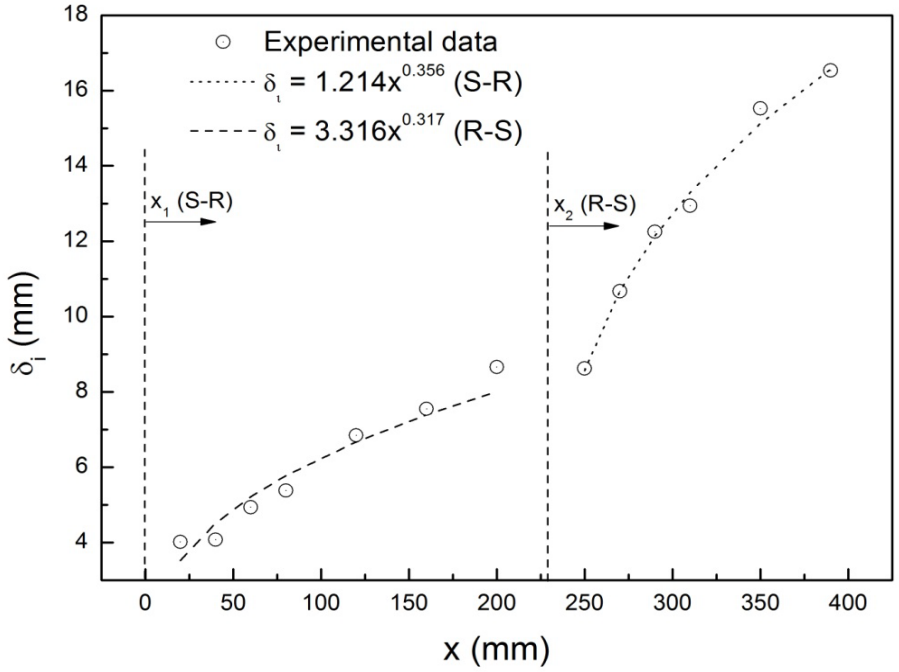


a)

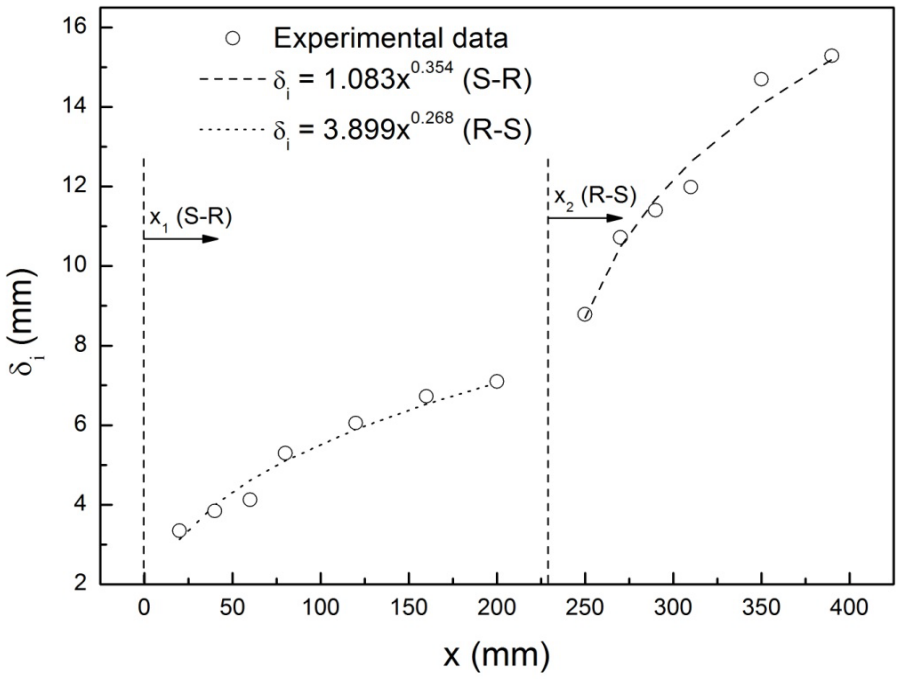


b)

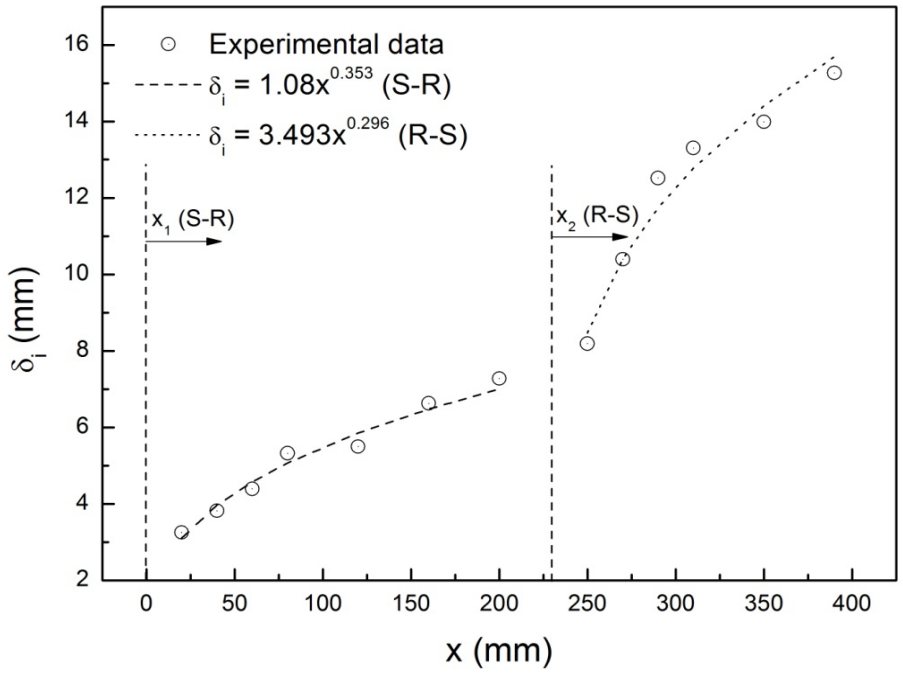


c)

Figure 5.6: Growth rate of the IBL thickness, a) $U_e$ = 20 m/s; b) $U_e$ = 30 m/s; c) $U_e$ = 40 m/s.

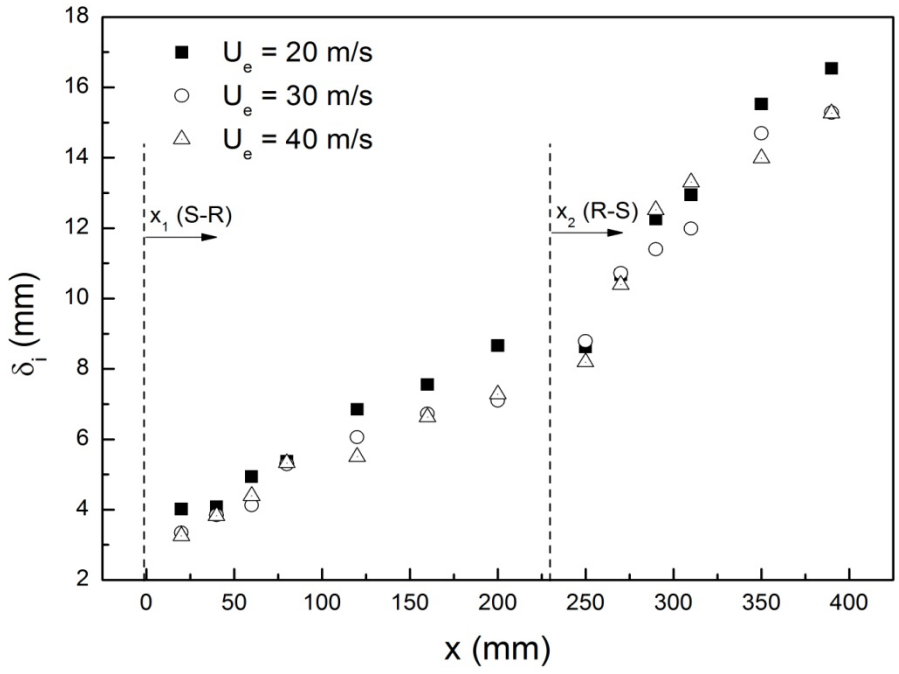


Figure 5.7: Development of the IBL thickness in the streamwise direction.

Figures 5.8 a) and b) represent the growth rates for the IBL over smooth-rough and rough-smooth transitions, respectively, scaled by the downwind roughness length, $z_{02}$. This means for the smooth-rough transition, $z_{02}$ is the roughness length of the rough surface, and for the rough-smooth transition, $z_{02}$ is the roughness length of the smooth surface. The definition of the roughness length, $z_0$, is the height above the displacement plane at which the mean wind becomes zero by extrapolating the logarithmic wind-speed profile downward through the surface layer. It is a theoretical height that must be determined from the wind-speed profile, and Monin-Obukhov similarity theory (Monin and Obukhov (1954)) can be used for estimating its value. Details of the Monin-Obukhov similarity theory are documented in Appendix B. Using this theory and fitting the mean velocity profiles to the data from the smooth and entirely rough surfaces, the roughness length, $z_0$, of the smooth and rough surfaces are obtained, respectively, i.e., $z_{0S}$ = 0.002 mm and $z_{0R}$ = 0.037 mm.

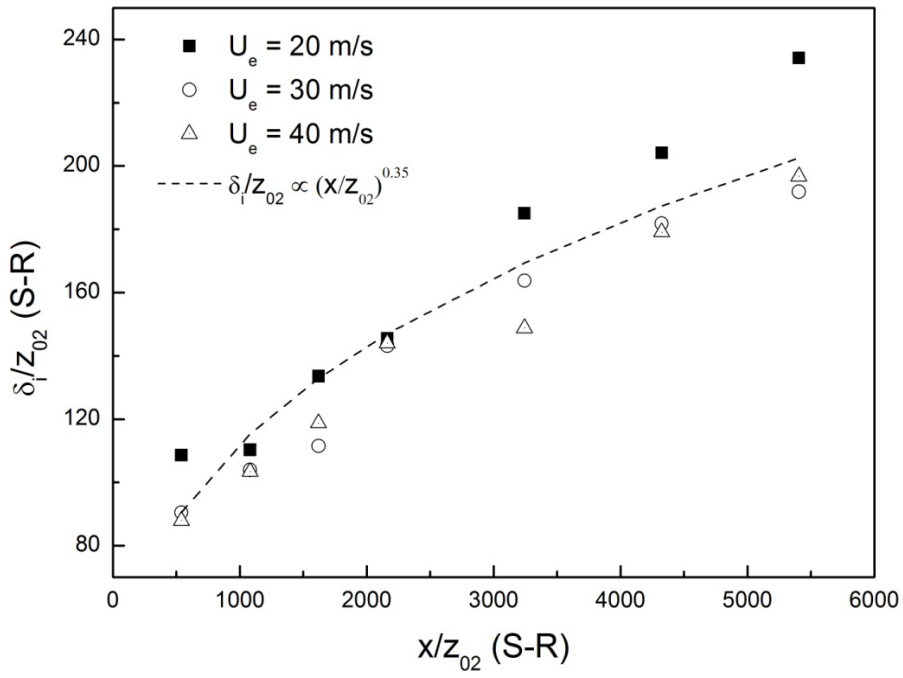


a)

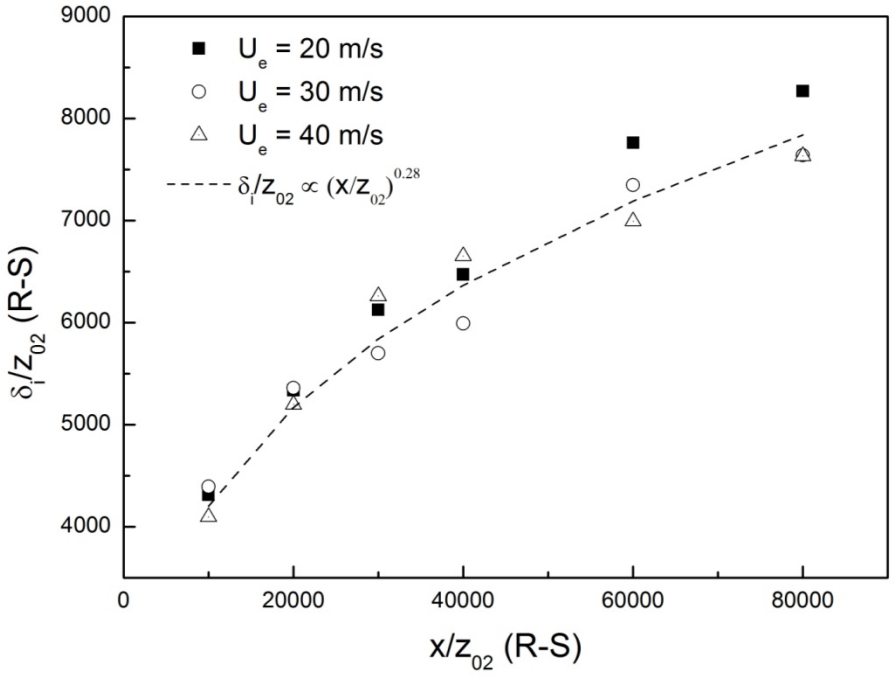


b)

Figure 5.8: Growth rate for the IBL thickness scaled by the roughness length, $z_{02}$:
a) Smooth-rough; b) Rough-smooth.

In this study, the growth rate of $\delta_i$ over the smooth-rough transition, i.e., $\frac{\delta_i}{z_{02}} \propto \left(\frac{x}{z_{02}}\right)^{0.35}$, is slower than that given by the theory of Elliott (1958), $\frac{\delta_i}{z_{02}} \propto \left(\frac{x}{z_{02}}\right)^{0.8}$ and the measurements of Antonia and Luxton (1971), $\frac{\delta_i}{z_{02}} \propto \left(\frac{x}{z_{02}}\right)^{0.72}$. The difference may be due to differences in the types of roughness used from their studies.

Furthermore, as shown in Figure 5.8, the growth rate of $\delta_i$ over the rough-smooth transition is proportional to $\left(\frac{x}{z_{02}}\right)^{0.28}$. This confirms the previous conclusion that the growth of $\delta_i$ over the rough-smooth transition is slower than that over a second smooth-rough transition. Meanwhile, it is also observed that this growth is slower than that over the single rough-smooth transition, i.e.,

$\frac{\delta_i}{z_{02}} \propto \left(\frac{x}{z_{02}}\right)^{0.43}$. This indicates that parts of the flow may still be influenced by the previous surface condition, and therefore, the flow is not in equilibrium with the local surface.

## 5.6 Summary

In this chapter, the development of the flow over a smooth-rough-smooth transition is investigated based on wind-tunnel measurements. The method of Antonia and Luxton (1971, 1972) is used to determine the IBL thickness, $\delta_i$ and the growth rate of $\delta_i$ is obtained along the streamwise direction. However, due to the insufficient near-wall resolution of the Pitot tube measurements, for the second surface transition, only the combined IBL with the first transition was investigated, and as such, the IBL only caused by the second transition was not considered here. The following summarizes major research approaches used and some of the preliminary conclusions:

(1) The characteristics of the flow over the smooth-rough-smooth transition are investigated through the streamwise development of the mean velocity profiles, displacement thickness, momentum thickness and shape factor.

(2) Using the method of Antonia and Luxton (1971, 1972), the values of the IBL thickness, $\delta_i$, for three different freestream velocities at different streamwise locations are obtained. It is observed that the growth rate of the IBL thickness is insensitive to the Reynolds number, and the grow rates of $\delta_i$ are similar for all three different freestream velocities.

(3) The results indicate that the growth of $\delta_i$ over the smooth-rough transition follows

$\frac{\delta_i}{z_{02}} \propto \left(\frac{x}{z_{02}}\right)^{0.35}$, which is smaller than that in previous study of Antonia and Luxton (1971), i.e., $\frac{\delta_i}{z_{02}} \propto \left(\frac{x}{z_{02}}\right)^{0.72}$. Meanwhile, it is confirmed that the growth of $\delta_i$ over smooth-rough transition is more rapid than that over a subsequent rough-smooth transition.

(4) The growth rate of $\delta_i$ over the rough-smooth transition in our case is slower than that over the single rough-smooth transition, indicating that parts of the flow may still be influenced by the previous surface condition, and so, the flow is not fully in equilibrium with the local downstream surface.

# 6 CONCLUSIONS AND DISCUSSIONS OF FUTURE WORK

## 6.1 Conclusions

In this thesis, the effects of roughness on a zero-pressure gradient turbulent boundary layer are investigated using an experimental method in a wind tunnel. Two aspects of the surface roughness effects are examined, including 1) the similarity between the smooth and rough turbulent boundary layers in terms of the defect velocity profile, and 2) the characteristics of the turbulent boundary layer after a step change in roughness.

To investigate the similarity between smooth- and rough-wall turbulent boundary layers, an analysis was performed based on experimental study of a smooth surface and several different rough surfaces using a theoretical derivation based on the assumption of complete similarity. An analytical equation has been derived to examine the validity of the outer velocity scaling for the mean velocity defect law proposed by Zagarola and Smits (1998) and the condition of similarity in the outer region of the boundary layer. The discussions and analysis of the results have been presented in Chapter 4, and major conclusions are summarized as follows

(1) From a thorough comparative study of the mean velocity defect profiles scaled by the friction velocity, $u_\tau$, the freestream velocity, $U_e$ and the ZS-scaling, $U_e \frac{\delta^*}{\delta}$, it confirms the widely accepted viewpoint that the ZS-scaling is the most effective outer scale for the

mean defect profile, and it successfully unifies the results based on different types of roughness.

(2) Through use of the new equation derived based on the assumption of complete similarity in the entire boundary layer, the ZS-scaling is found to be an effective scale for assessing similarity between different types of rough surfaces over the entire boundary layer and also similarity between the smooth and rough surfaces in the outer region. However, it does not collapse the profiles in the region from $y = 0$ to $y = 0.4\delta$, which includes the inner layer, the overlap region and part of the outer region. This conclusion challenges the widely accepted viewpoint that the ZS-scaling is an effective scale for the mean velocity defect profiles in both the overlap and outer regions.

(3) The failure of the ZS-scaling in collapsing the mean defect profiles in the region from $y = 0$ to $y = 0.4\delta$ suggests that similarity does not exist in this region and the effects of the roughness extend into the outer region (instead of being confined to the inner layer). Furthermore, the similar behavior observed for different types of rough surfaces indicates that for the fully rough surfaces, the roughness elements of different roughness geometries have similar effects on the structure of the turbulent boundary layer.

(4) Comparisons of different Reynolds numbers further confirm the previous conclusion that the ZS-scaling can indeed eliminate the effects of Reynolds numbers on the similarity of turbulent boundary layers.

The characteristics of the boundary layer flowing over a step change in roughness step have also been investigated experimentally. Sand papers were used to create fully rough transitions, and

the mean velocity profiles at different locations were measured using a boundary layer Pitot tube. The method of Antonia and Luxton (1971, 1972) was applied to calculation of the IBL thickness, $\delta_i$. Based on the value of $\delta_i$, the growth rates along the streamwise direction were evaluated. Detailed analysis of the results have been presented in Chapter 5, and major conclusions of this research are summarized in the following context:

(1) The mean velocity profiles clearly demonstrate the development of the flow after the two consecutive step changes in roughness.

(2) Using the method of Antonia and Luxton (1971, 1972), the values of the IBL thickness, $\delta_i$, for three different freestream velocities at different streamwise locations are obtained. It is observed that the growth rate of the IBL thickness is insensitive to the Reynolds number, and the grow rates of $\delta_i$ are similar for all three different freestream velocities.

(3) The results indicate that the growth of $\delta_i$ over the smooth-rough transition follows $\frac{\delta_i}{z_{02}} \propto \left(\frac{x}{z_{02}}\right)^{0.35}$, which is smaller than that in previous study of Antonia and Luxton (1971), i.e., $\frac{\delta_i}{z_{02}} \propto \left(\frac{x}{z_{02}}\right)^{0.72}$. Meanwhile, it is confirmed that the growth of $\delta_i$ over smooth-rough transition is more rapid than that over a subsequent rough-smooth transition.

(4) The growth rate of $\delta_i$ over the rough-smooth transition in our case is slower than that over a single rough-smooth transition, indicating that parts of the flow may still be influenced by the previous surface condition, and so, the flow is not fully in equilibrium with the local downstream surface.

## 6.2 Discussions of the Future Work

In this thesis, both theoretical and experimental methods have been used to investigate the similarity between the smooth and rough turbulent boundary layers and the flow over a set of two step changes in roughness. The results in this thesis not only confirm the previous commonly accepted conclusions, but also challenge the classical viewpoint in the field of turbulent research. However in order to obtain a deeper insight into these subjects, some recommendations for future investigation are given as follows:

(1) To further validate the new method based on the analytical equation presented in Chapter 4, more data from different types of rough surfaces and Reynolds numbers are needed. Furthermore, some more precise measurement methods are required to achieve a better near-wall resolution, which would subsequently increase the accuracy in the calculation of the friction velocity, $u_\tau$.

(2) To further explore the characteristics of turbulent boundary layers over step changes in roughness, the local value of the friction velocity, $u_\tau$, along the streamwise direction is required. Since the flow is not fully developed after the step change in roughness, the method of profile fitting to the Log Law is not suitable for determining the value of $u_\tau$. Therefore, further improved methods are needed for more precise determination of the development of $u_\tau$ over the step change in roughness. If the value of the friction velocity can be more accurately determined, the characteristics of the flow over the step change in roughness will be better understood.

(3) The study on the development of the IBL over the second step change in roughness needs to be further refined. For the present experimental configuration, the IBL after the rough-smooth transition is actually composed by two parts: a new IBL is created due to the new surface, which develops within the “old” IBL created by the previous smooth-rough transition. Future experimental should give a priority to using refined near-wall measurements to resolve the characteristics of the second IBL. Furthermore, additional measurements of Reynolds shear stresses are required to further investigate the characteristics of IBL by the definition of turbulent components.

# REFERENCES


Akinlade, O. G., Bergstrom, D. J., Tachie, M. F., & Castillo, L. (2004). Outer flow scaling of smooth and rough wall turbulent boundary layers. *Experiments in Fluids*, *37*(4), 604-612.

Akinlade, O. G. (2005). *Effects of surface roughness on the flow characteristics in a turbulent boundary layer*, Doctoral dissertation, University of Saskatchewan.

Antonia, R. A., & Luxton, R. E. (1971). The response of a turbulent boundary layer to a step change in surface roughness. Part 1. Smooth to rough. *Journal of Fluid Mechanics*, *48*(04), 721-761.

Antonia, R. A., & Luxton, R. E. (1972). The response of a turbulent boundary layer to a step change in surface roughness. Part 2. Rough to smooth. *Journal of Fluid Mechanics*, *53*(04), 737-757.

Bergstrom, D. J., Kotey, N. A., & Tachie, M. F. (2002). The effects of surface roughness on the mean velocity profile in a turbulent boundary layer. *Journal of Fluids Engineering*, *124*(3), 664-670.

Bradley, E. F. (1968). A micrometeorological study of velocity profiles and surface drag in the region modified by a change in surface roughness. *Quarterly Journal of the Royal Meteorological Society*, *94*(401), 361-379.

Brzek, B., Cal, R. B., Johansson, G., & Castillo, L. (2007). Inner and outer scalings in rough surface zero pressure gradient turbulent boundary layers. *Physics of Fluids*, *19*(6), 065101.

Castillo, L., & George, W. K. (2001). Similarity analysis for turbulent boundary layer with pressure gradient: outer flow. *AIAA Journal*, *39*(1), 41-47.

Chamorro, L. P., & Porté-Agel, F. (2009). Velocity and surface shear stress distributions behind a rough-to-smooth surface transition: a simple new model. *Boundary-Layer Meteorology*, *130*(1), 29-41.

Cheng, H., & Castro, I. P. (2002). Near-wall flow development after a step change in surface roughness. *Boundary-Layer Meteorology*, *105*(3), 411-432.

Clauser, F. H. (2012). Turbulent boundary layers in adverse pressure gradients. *Journal of the Aeronautical Sciences (Institute of the Aeronautical Sciences)*, *21*(2).

Coleman, H. W., & Steele, W. G. (2009). *Experimentation, validation, and uncertainty analysis for engineers*. John Wiley & Sons.

Connelly, J. S., Schultz, M. P., & Flack, K. A. (2006). Velocity-defect scaling for turbulent boundary layers with a range of relative roughness. *Experiments in Fluids*, *40*(2), 188-195.

Efros, V., & Krogstad, P. Å. (2011). Development of a turbulent boundary layer after a step from smooth to rough surface. *Experiments in Fluids*, *51*(6), 1563-1575.

Elliott, W. P. (1958). The growth of the atmospheric internal boundary layer. *Transactions, American Geophysical Union*, *39*, 1048-1054.

Flack, K. A., Schultz, M. P., & Shapiro, T. A. (2005). Experimental support for Townsend's Reynolds number similarity hypothesis on rough walls. *Physics of Fluids*, *17*(3), 035102.

Furuya, Y., & Fujita, H. (1967). Turbulent boundary layers on wire-screen roughnesses. *Bulletin of JSME*, *10*(37), 77-86.

Garratt, J. R. (1990). The internal boundary layer—a review. *Boundary-Layer Meteorology*, *50*(1-4), 171-203.

George, W. K., & Castillo, L. (1997). Zero-pressure-gradient turbulent boundary layer. *Applied Mechanics Reviews*, *50*(12), 689-729.

Glendening, J. W., & Lin, C. L. (2002). Large eddy simulation of internal boundary layers created by a change in surface roughness. *Journal of the Atmospheric Sciences*, *59*(10), 1697-1711.

Hama, F. R. (1954). *Boundary-layer characteristics for smooth and rough surfaces*. Society of Naval Architects and Marine Engineers (SNAME).

Jackson, N. A. (1976). The propagation of modified flow downstream of a change in roughness. *Quarterly Journal of the Royal Meteorological Society*, *102*(434), 924-933.

Jegede, O. O., & Foken, T. H. (1999). A study of the internal boundary layer due to a roughness change in neutral conditions observed during the LINEX field campaigns. *Theoretical and Applied Climatology*, *62*(1-2), 31-41.

Jensen, N. O. (1978). Change of surface roughness and the planetary boundary layer. *Quarterly Journal of the Royal Meteorological Society*, *104*(440), 351-356.

Jiménez, J. (2004). Turbulent flows over rough walls. *Annual Review of Fluid Mechanics*, 36, 173-196.

Keirsbulck, L., Labraga, L., Mazouz, A., & Tournier, C. (2002). Surface roughness effects on turbulent boundary layer structures. *Journal of Fluids Engineering*, *124*(1), 127-135.

Krogstad, P. Å., Antonia, R. A., & Browne, L. W. B. (1992). Comparison between rough-and smooth-wall turbulent boundary layers. *Journal of Fluid Mechanics*, *245*, 599-617.

Krogstadt, P. Å., & Antonia, R. A. (1999). Surface roughness effects in turbulent boundary layers. *Experiments in Fluids*, *27*(5), 450-460.

Laursen, T. S., Fredsøe, J., & Sumer, B. M. (1994). Numerical prediction of wave boundary layer over a bed with a change in roughness. *Coastal Engineering*, *24*(1), 81-96.

Logan, E., & Fichtl, G. H. (1975). Rough-to-smooth transition of an equilibrium neutral constant stress layer. *Boundary-Layer Meteorology*, *8*(3), 525-528.

Millikan, C. B. (1938). A critical discussion of turbulent flows in channels and circular tubes. *Fifth International Congress for Applied Mechanics* (Vol. 386).

Monin, A. S., & Obukhov, A. (1954). Basic laws of turbulent mixing in the surface layer of the atmosphere. *Contributions of the Geophysical Institute of the Slovak Academy of Sciences USSR*, *151*, 163-187.

Panofsky, H. A., & Townsend, A. A. (1964). Change of terrain roughness and the wind profile. *Quarterly Journal of the Royal Meteorological Society*, *90*(384), 147-155.

Panofsky, H. A., & Dutton, J. A. (1984). *Atmospheric turbulence, models and methods for engineering applications.* New York: Wiley.

Patel, V. C. (1998). Perspective: flow at high Reynolds number and over rough surfaces—Achilles heel of CFD. *Journal of Fluids Engineering*, *120*(3), 434-444.

Pendergrass, W., & Arya, S. P. S. (1984). Dispersion in neutral boundary layer over a step change in surface roughness—I. Mean flow and turbulence structure. *Atmospheric Environment*, *18*(7), 1267-1279.

Perry, A. E., Schofield, W. H., & Joubert, P. N. (1969). Rough wall turbulent boundary layers. *Journal of Fluid Mechanics*, *37*(02), 383-413.

Perry, A. E., & Abell, C. J. (1977). Asymptotic similarity of turbulence structures in smooth-and rough-walled pipes. *Journal of Fluid Mechanics*, *79*(04), 785-799.

Peterson, E. W. (1969). Modification of mean flow and turbulent energy by a change in surface roughness under conditions of neutral stability. *Quarterly Journal of the Royal Meteorological Society*, *95*(405), 561-575.

Pope, S. B. (2000). *Turbulent flows*. Cambridge university press.

Rao, K. S., Wyngaard, J. C., & Coté, O. R. (1974). The structure of the two-dimensional internal boundary layer over a sudden change of surface roughness. *Journal of the Atmospheric Sciences*, *31*(3), 738-746.

Raupach, M. R., Antonia, R. A., & Rajagopalan, S. (1991). Rough-wall turbulent boundary layers. *Applied Mechanics Reviews*, *44*(1), 1-25.

Savelyev, S. A., & Taylor, P. A. (2001). Notes on an internal boundary-layer height formula. *Boundary-Layer Meteorology*, *101*(2), 293-301.

Savelyev, S. A., & Taylor, P. A. (2005). Internal boundary layers: I. Height formulae for neutral and diabatic flows. *Boundary-Layer Meteorology*, *115*(1), 1-25.

Schlichting, H. (1979). *Boundary Layer Theory*. McGraw-Hill, New York.

Seo, J., Castillo, L., Johansson, T. G., & Hangan, H. (2004). Reynolds stress in turbulent boundary layers at high Reynolds number. *Journal of Turbulence*, *5*, 13-13.

Shir, C. C. (1972). A numerical computation of air flow over a sudden change of surface roughness. *Journal of the Atmospheric Sciences*, *29*(2), 304-310.

Tachie, M. F., Bergstrom, D. J., & Balachandar, R. (2000). Rough wall turbulent boundary layers in shallow open channel flow. *Journal of Fluids Engineering*, *122*(3), 533-541.

Tachie, M. F., Bergstrom, D. J., & Balachandar, R. (2003). Roughness effects in low-Reθ open-channel turbulent boundary layers. *Experiments in Fluids*, *35*(4), 338-346.

Townsend, A. A. (1980). *The structure of turbulent shear flow*. Cambridge university press.

Weng, W., Taylor, P. A., & Salmon, J. R. (2010). A 2-D numerical model of boundary-layer flow over single and multiple surface condition changes. *Journal of Wind Engineering and Industrial Aerodynamics*, *98*(3), 121-132.

Weyburne, D. W. (2008). *The Mathematics of Flow Similarity of the Velocity Boundary Layer* (No. AFRL-RY-HS-TR-2010-0014). Sensors Directorate/Electromagnetics Technology Division, Air Force Research Lab, Hanscom AFB Ma.

Wood, D. H. (1982). Internal boundary layer growth following a step change in surface roughness. *Boundary-Layer Meteorology*, *22*(2), 241-244.

Zagarola, M. V., & Smits, A. J. (1998). Mean-flow scaling of turbulent pipe flow. *Journal of Fluid Mechanics*, *373*, 33-79.

# APPENDIX A

## Uncertainty Analysis

In order to perform an uncertainty analysis (based on a 95 %) estimate and bias confidence limits, the procedure suggested by Coleman and Steele (1999) was used. The uncertainty estimate of the freestream velocity is determined by

$$U_e = \sqrt{\frac{2\Delta P}{\rho}}$$

where $\Delta P$ is the dynamic pressure and $\rho$ is the air density. The bias and precision errors of the dynamic pressure were given by the manufacturer in the pressure transducer manual: $B_{\Delta P}^2 =$ 0.35 % and $P_{\Delta P}^2 = 0.98$ %. As such, the uncertainty estimate of the dynamic pressure is

$$U_{\Delta P}^C = \sqrt{B_{\Delta P}^2 + P_{\Delta P}^2} = \pm 1.04\%$$

Assuming that the air is an ideal gas, then the air density can be determined by

$$\rho = \frac{P_a}{RT}$$

where $P_a$ is the absolute pressure, $R$ is the gas constant, and $T$ is the absolute temperature. Based on this equation, the uncertainty estimate of the air density can be determined as

$$\frac{U_\rho}{\rho} = \left[ \left( \frac{U_{P_a}}{P_a} \right)^2 + \left( \frac{U_T}{T} \right)^2 \right]^{1/2}$$

Because uncertainty estimates of the absolute pressure and temperature are 0.99 % and 0.33 %, respectively, the uncertainty estimate of the air density is

$$\frac{U_\rho}{\rho} = \left[ (0.99)^2 + (0.33)^2 \right]^{1/2} = \pm 1.08\ \%$$

Therefore, the uncertainty estimate of the freestream velocity, $U_e$, is

$$\frac{U_{U_e}^C}{U_e} = \left[ \left( \frac{1}{2} \frac{U_{\Delta P}^C}{\Delta P} \right)^2 + \left( \frac{1}{2} \frac{U_\rho^C}{\rho} \right)^2 \right]^{1/2} = \pm 0.75\ \%$$

# APPENDIX B

## The Roughness Length $z_0$

The definition of the roughness length, $z_0$, is the height above the displacement plane at which the mean wind becomes zero based on the extrapolation of the logarithmic velocity profile downwards through the boundary layer. It is a theoretical height that must be determined from the wind-speed profile.

The Monin-Obukhov similarity theory (Monin and Obukhov (1954)) can be used to determine the value of $z_0$, which states

$$\overline{M} = \frac{u_*}{\kappa}\left[\ln\left(\frac{z-d}{z_0}\right) + \Psi\left(\frac{z-d-z_0}{L}\right)\right]$$

where $\bar{M}$ is the average wind speed, and $\Psi = 0$ if the flow is neutrally stratified.

In order to determine $z_0$, the mean velocity profile is fitted to the following equation:

$$\overline{M} = \frac{u_*}{\kappa}\ln\left(\frac{z-d}{z_0}\right)$$

Where $d$ is the height of the displacement plane above ground.

After fitting the mean velocity profiles to the data for the smooth and fully rough surfaces, the roughness length $z_0$ of the smooth and rough surfaces can be determined, respectively, with $z_{0S}$ = 0.002 mm and $z_{0R}$ = 0.037 mm.